Shear thinning and shear dilatancy of liquid n -hexadecane via equilibrium and nonequilibrium molecular dynamics simulations: Temperature, pressure, and density effects

Huan-Chang Tseng, Jiann-Shing Wu, and Rong-Yeu Chang

Articles you may be interested in

Master curves and radial distribution functions for shear dilatancy of liquid n -hexadecane via nonequilibrium molecular dynamics simulations
J. Chem. Phys. 130, 164515 (2009); 10.1063/1.3123171

Material functions of liquid n -hexadecane under steady shear via nonequilibrium molecular dynamics simulations: Temperature, pressure, and density effects
J. Chem. Phys. 130, 084904 (2009); 10.1063/1.3080768

Transport properties of C O 2 -expanded acetonitrile from molecular dynamics simulations
J. Chem. Phys. 126, 074507 (2007); 10.1063/1.2434968

Molecular simulation of dendrimers and their mixtures under shear: Comparison of isothermal-isobaric (N p T) and isothermal-isochoric (N V T) ensemble systems
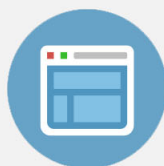J. Chem. Phys. 123, 034905 (2005); 10.1063/1.1946749

Nonequilibrium properties of linear polar Kihara fluids from molecular dynamics. Results for models and for liquid acetonitrile
J. Chem. Phys. 107, 2034 (1997); 10.1063/1.474554

Shear thinning and shear dilatancy of liquid *n*-hexadecane via equilibrium and nonequilibrium molecular dynamics simulations: Temperature, pressure, and density effects

Huan-Chang Tseng,[1] Jiann-Shing Wu,[1,a)] and Rong-Yeu Chang[2]

[1]*Department of Applied Chemistry, National Chiao Tung University, Hsinchu, Taiwan 30010, Republic of China*

[2]*Department of Chemical Engineering, National Tsing Hua University, Hsinchu, Taiwan 30043, Republic of China*

Equilibrium and nonequilibrium molecular dynamics (MD) simulations have been performed in both isochoric-isothermal (*NVT*) and isobaric-isothermal (*NPT*) ensemble systems. Under steady state shearing conditions, thermodynamic states and rheological properties of liquid *n*-hexadecane molecules have been studied. Between equilibrium and nonequilibrium states, it is important to understand how shear rates ($\dot{\gamma}$) affect the thermodynamic state variables of temperature, pressure, and density. At lower shear rates of $\dot{\gamma} < 1 \times 10^{11}$ s^{-1}, the relationships between the thermodynamic variables at nonequilibrium states closely approximate those at equilibrium states, namely, the liquid is very near its Newtonian fluid regime. Conversely, at extreme shear rates of $\dot{\gamma} > 1 \times 10^{11}$ s^{-1}, specific behavior of *shear dilatancy* is observed in the variations of nonequilibrium thermodynamic states. Significantly, by analyzing the effects of changes in temperature, pressure, and density on shear flow system, we report a variety of rheological properties including the *shear thinning* relationship between viscosity and shear rate, zero-shear-rate viscosity, rotational relaxation time, and critical shear rate. In addition, the flow activation energy and the pressure-viscosity coefficient determined through Arrhenius and Barus equations acceptably agree with the related experimental and MD simulation results. © *2008 American Institute of Physics.* [DOI: 10.1063/1.2943314]

I. INTRODUCTION

An in-depth understanding of ultrathin films at the atomic level is important in probing the behavior of fluids with respect to variations of thermodynamics states and rheological properties, especially for nanolubrication or nanotribological processes. Oftentimes, the surface force apparatus[1,2] (SFA), which can directly measure thicknesses and frictional forces, or van der Waals (vdW) forces between two mica surfaces, has been widely used in lubrication unit to study the thin film's viscosity on atomic and molecular scales. When using the SFA, the layer thickness of ultrathin is at approximately 2.4 nm or about six molecule layers.[3] In such lubrication experiments, liquid *n*-hexadecane is one of the more commonly used fluids.[2–4]

In recent years, molecular dynamics (MD) simulation has explicitly become a standard tool in the prediction of macroscopic properties and observed microscopic behaviors for analytical computer experiments of fluid behaviors. MD simulation can be classified into two major types, namely, equilibrium molecular dynamics (EMD) and nonequilibrium molecular dynamics (NEMD) simulations. EMD simulation,[5] based on Newton's laws of motion, describes various molecular motions of fluid at equilibrium state. In general, by using the Green–Kubo (GK) relation[5–8] in EMD simulation, the zero-shear-rate viscosity of liquid molecules can be easily calculated. Specifically, in studies of fluids with long molecular chains, the time executed to reach equilibrium condition must be quite long. So far, the limitation on run length[8] is over 1×10^{-8} time steps (about 13.1 ns) when utilizing the GK relation for 100 *n*-hexadecane molecules.[6] Thus, the EMD simulation combining the GK relation becomes an economically impractical method, since fluids with long molecular chain require many statistical samples and significant computational resources to predict the zero-shear-rate viscosity.

At present, NEMD simulations have been applied in the practical lubrication process[9] to estimate the fluid's viscosity. NEMD simulation, dominated by SLLOD equations[10–12] of motion, can realistically describe shear[13,14] and elongation[15,16] flows. Until now, few NEMD studies have been used to analyze rheological properties in the small-amplitude oscillation shear flow[17] and the stress growth upon inception shear flow.[18] Therefore, NEMD simulation is a widely used numerical method for the prediction of rheological properties of fluids. Basically, the extrapolated zero-shear-rate viscosity[8,14,19,20] is obtained at low shear rates by NEMD simulation of the viscosity–shear rate relationship, which contains the first Newtonian region and shear thinning region. Early development of NEMD simulation[14,21] for simple gases of argon (Ar) calculated rheological properties by Lennard–Jones (LJ) or Weeks–Chandler–Andersen

a)Author to whom correspondence should be addressed. Tel.: 886-3-5712121, ext. 31520. FAX: 886-3-5723764. Electronic mail: inblue.ac89g@nctu.edu.tw. Present address: Science Building 2, 1001 Ta Hsueh Road, Hsinchu, Taiwan 30010, Republic of China.

129, 014502-1

(WCA) potentials. In NEMD studies,[19,22–31] shear dilatancy and shear thinning behaviors are often observed nonlinear behaviors through the variations of thermodynamic states and viscosities with shear rates, respectively. At high shear rates, the dependence of pressure or density on shear rate is known as shear dilatancy.[22] In non-Newtonian fluids we comprehend the phenomenon of shear thinning, which indicates that the viscosity decreases with an increase in shear rate. On a macroscopic scale, Ar fluid generally behaves like a Newtonian fluid. Unexpectedly, on a microscopic scale, Ar fluid also exhibits shear thinning behavior and nonzero normal stress differences.[14] At extreme shear rates over 1 $\times 10^{13}$ s^{-1}, shear thickening,[21] in which the viscosity increases while shear rate abidingly increases, occurs abruptly. It obviously shows that microscopic fluid behaviors can vary significantly from our macroscopic knowledge of fluid behaviors.

As will be further described in the ensuing NEMD discussion[10,23,28,31–39] via realistic molecular potentials for many n-alkane molecules, the zero-shear-rate viscosities analyzed at various thermodynamic states[36–39] were shown to match closely when compared to experimental results. Significantly, there was an important finding[37] in which NEMD simulation and experimental data were shown to follow the same time-temperature superposition master curve.

In addition, some NEMD researches[24,40,41] using the finite extensible nonlinear elastic (FENE) potential[24,27,40–44] have described the segmental motion of chains to analyze the relationship between the zero-shear-rate viscosity (η_0) and the molecular weight (M) for linear chain molecules. Consequently, this $\eta_0 - M$ relationship presents that the crossover point[24,40,41] from $\eta_0 \propto M^1$ to $\eta_0 \propto M^{3.0-3.5}$ corresponds to the transition of polymer dynamic theory from the Rouse model regime to the repatation model regime. These results are in agreement with theoretical[45,46] and experimental[47–49] results. In terms of linear and branch isomeric structures,[31,35] the influence of molecular structures on the rheological properties reveals that the degree of increase in the number of molecular branches corresponds to an increase in viscosity, which is also consistent with experimental results.

The primary factors affecting viscosity are changes of thermodynamic states, namely, temperature, pressure, and density, as well as molecular structure and weight.[47–49] In practice, most rheological experiments[48] are measured under the conditions of *constant temperature* and *pressure*. In rheological computational technology, NEMD simulation algorithms contain two analytical systems, constant volume/isochoric-isothermal (*NVT*-NEMD) and constant pressure/isobaric-isothermal (*NPT*-NEMD) systems. Most NEMD simulation studies were performed in the *constant volume* system to compare with previous related rheological experimental studies. In contrast, there is little information on the particular investigative topic of using constant pressure NEMD (Refs. 25–27, 30, 43, and 50) simulation. Regrettably, by using constitutive equations of fluid mechanics[47–49] and kinetic theory[45,46,51] of liquid polymers, the temperature, pressure, and density effects cannot be directly understood. Constitutive equations must cooperate with Arrhenius[49] or Williams–Landel–Ferry[52] (WLF) equations to describe the

temperature effect and combine with Barus equation[9,36] to describe the pressure effect. Therefore, for the temperature and pressure effects, the understanding of the changes in the rheological properties can be indirectly analyzed. Additionally, the variations in viscosities with respect to volume or density are explained through Doolittle's free volume concept.[52]

As a review of the literatures above suggests that many studies about rheological properties of n-hexadecane molecules[13,19,34,53,54] have been reported by using constant volume NEMD simulation. Complete analyses of the temperature and pressure effects on shear thinning and shear dilatancy behaviors have not been discussed. Therefore it is the objective of the present study to understand those behaviors using both *NVT*-NEMD and *NPT*-NEMD simulations for various thermodynamic states, including pressure-volume-temperature *P-V-T* data and shear dilatancy behavior, and rheological properties, including the shear thinning relationship between viscosity and shear rate, zero-shear-rate viscosity, rotational relaxation time, and critical shear rate.

The rest of the paper is organized as follows. In Sec. II, the details of molecular models and potentials, simulation methods, and statistic properties are described. In Sec. III, the simulation results comparing two different potential models are exhibited, and the agreements of *NPT*-NEMD simulation with *NVT*-NEMD simulation are verified. From a thermodynamics perspective, we should understand how thermodynamic state *P-V-T* data are influenced by shear rates, as well as observe the variation of shear dilatancy at high shear rates. From a rheological perspective, this study explores how the variation of shear thinning in constant pressure NEMD simulation is separately induced by the pressure and temperature effects. Moreover, the flow activation energy of Arrhenius equation and the viscosity-pressure coefficient of Barus equation are calculated for liquid n-hexadecane, respectively. The change in shear thinning with various densities using constant volume NEMD simulation is also investigated. Specifically, Doolittle's free volume concept is adopted to explain the changes in viscosity under various pressures, temperatures, and densities. In the final section, we present main conclusions and make suggestions for further studies.

II. SIMULATION DETAILS

To understand the changes in thermodynamic states and rheological properties, NEMD simulations for liquid n-hexadecane are presented. The simulation details can be broken into three parts: (1) molecular modeling and potential models of n-hexadecane molecular chains, (2) simulation algorithms containing equations of motion and their numerical methods, and (3) definition of statistical properties of temperature, pressure, and viscosity.

A. Potential models

An n-hexadecane molecular chain is a linear chain of molecules. The structure and characteristics of a linear molecular chain are shown graphically in Fig. 1 below. As shown in the figure,[55] the molecular chain is modeled using
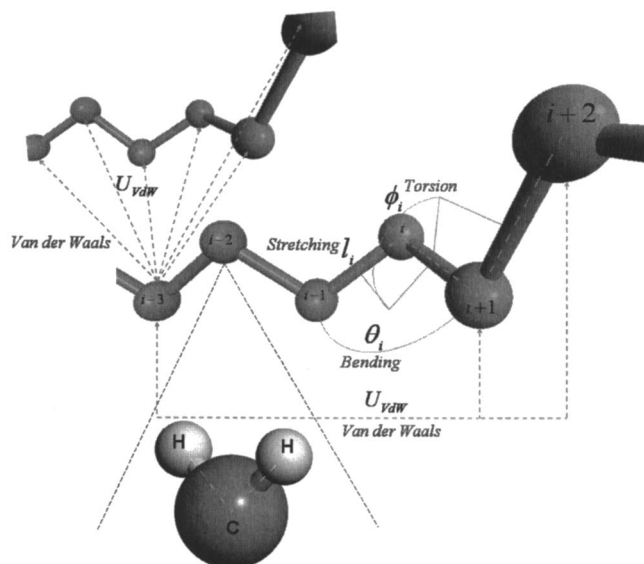
FIG. 1. The model of a linear molecular chain consists of CH_2 groups, which are considered spherical interaction sites. The basic features of the bonding interaction can be described by stretching, bending, and torsion motions. van der Waals interactions occur between CH_2 groups of different chains and also between CH_2 groups in the same chain separated by more than three CH_2 groups.

spherical interaction sites, regarded as CH_2 groups. Connected interaction sites will combine together to form molecular chains. This type of molecular chain model is known as the united atom (UA), which is widely used for the simulation of alkane, hexadecane, and polyethylene molecular chains. The flexibility of molecular chains is dominated by the total potential U_{tot}, which is comprised of bond stretching U_s, bond bending U_b, torsion U_t, and nonbonding (van der Waals potential U_{vdW}) interactions between CH_2 groups,

$$U_{tot} = U_{vdW} + U_s + U_b + U_t. \tag{1}$$

Two commonly used molecular potential models are described below as models A and B. First, Michopoulos and co-workers have fitted optimal parameters of the van der Waals potential[19,20] in predicted rheological properties cooperated with the stretching and bending potentials of White and Bovill[56] and combined the torsion potential of Ryckaert and Bellemans.[57] This set of potentials[20] has been denoted as model A in this study. Model A has been applied in the shear flow[53] and contraction flow[55] portions of MD simulation. Second, Martin and Siepmann has developed the transferable potential for phase equilibria (TraPPE) model,[58] which is an adaptation in calculating the vapor-liquid coexistence curve[59,60] and the surface tension[61] of n-alkane phase diagrams. This potential model is referred to as model B. All parameters for the two potential models are listed in Tables I and II. Notably, the shifted Lennard–Jones potential, which is equal to zero at a truncated point, can generally describe the vdW interaction between molecules. Thus, physical quantities are of course affected by the LJ potential truncation. Particularly for large intermolecular distances, when the shifted LJ potential is used, long-range corrections[62] must be added to both internal energy and pressure during the MD simulation procedure.

TABLE I. Covalent bonding interaction parameters for both potential models A and B.

		Model A[a]	Model B[b]	Units
Bond stretching	k_l	2650.98	3762.24	kJ mol^{-1} Å^{-2}
	l_0	1.53	1.54	Å
Bond bending	k_θ	0.1004	0.1582	kJ mol^{-1} deg^{-2}
	k'_θ	0.0096	$\cdots$	deg^{-1}
	θ_0	109.47	114.0	deg
Torsion	c_0	9.278	$\cdots$	kJ mol^{-1}
	c_1	12.155	2.949	kJ mol^{-1}
	c_2	-13.119	-0.566	kJ mol^{-1}
	c_3	-3.060	6.573	kJ mol^{-1}
	c_4	26.239	$\cdots$	kJ mol^{-1}
	c_5	-31.493	$\cdots$	kJ mol^{-1}

[a]Equilibrium bond length and bond angle (l_0 and θ_0) are taken from Ref. 20; bond stretching and bond bending force constants (k_l, k_θ, and k'_θ) are taken from Ref. 56; and torsion potential parameters are taken from Ref. 57.
[b]Taken from Ref. 58.

1. Model A

Model A only has one UA, namely, CH_2 groups. The vdW potential can occur in two different interactions between CH_2 groups. First, the vdW potential influences two CH_2 groups in the same molecular chain when two CH_2 groups are separated by at least three CH_2 groups. Second, the vdW potential affects two CH_2 groups in two different molecular chains. The vdW potential can be represented by the 12-6 LJ potential[19]

$$U_{LJ} = 4\varepsilon_{ij}\left[\left(\frac{\sigma_{ij}}{r_{ij}}\right)^{12} - \left(\frac{\sigma_{ij}}{r_{ij}}\right)^6\right], \tag{2}$$

where r_{ij} is the distance between two CH_2 groups, ε_{ij} and σ_{ij} are the energy and length parameters of the LJ potential, respectively, for the pair of groups i and j. To reduce computational time of the LJ force, the LJ potential is usually truncated at a cutoff distance r_c so that $U_{LJ}(r_c)=0$.

The bond stretching potential[56] connects two CH_2 groups by Hooke's harmonic potential

$$U_s = \frac{1}{2}k_l(l_i - l_0)^2, \tag{3}$$

where k_l is the bond stretching energy constant, l_0 is an equilibrium bond length, and l_i is the bond length between groups $i-1$ and i.

The bond bending potential[56] is described by the Taylor series' cubic term expansion of bending angle deviation,

TABLE II. Lennard–Jones interaction parameters for both potential models A and B.

	United atom	σ (Å)	ε (kJ mol^{-1})	r_c (Å)
Model A[a]	CH_2	4.045	0.420	9.0
Model B[b]	CH_2	3.950	0.382	11.5
	CH_3	3.750	0.814	

[a]Taken from Ref. 19.
[b]Taken from Ref. 58.

$$U_b = \tfrac{1}{2}k_\theta[(\theta_i - \theta_0)^2 - k'_\theta(\theta_i - \theta_0)^3], \tag{4}$$

where k_b is the bond bending energy constant, k'_θ is the bond bending angle constant, θ_0 is an equilibrium bond angle, and θ_i is a bond angle among three adjacent CH_2 groups $i-1$, i, and $i+1$.

The torsion potential[57] is expressed by a fifth-order cosine polynomial of a dihedral angle,

$$U_t = c_0 + c_1 \cos \phi_i + c_2 \cos^2 \phi_i + c_3 \cos^3 \phi_i + c_4 \cos^4 \phi_i$$
$$+ c_5 \cos^5 \phi_i, \tag{5}$$

where $\{c_n\}$ are the values of the set of torsion energy coefficients, and ϕ_i is the dihedral angle formed by four consecutive CH_2 groups $i-1$, i, $i+1$, and $i+2$.

2. Model B

Model B contained two UA groups, a CH_2 group and a CH_3 group. The functional forms of the LJ potential and stretching potential of model B are the same as those of model A, as shown in Eqs. (2) and (3). The Lorentz–Berthelot combining rules[31,58] for the LJ potential, $\sigma_{ij} = (\sigma_{ii} + \sigma_{jj})/2$ and $\varepsilon_{ij} = (\varepsilon_{ii}\varepsilon_{jj})^{1/2}$, are used for assessing the energy and length parameters of *unlike* UA interactions, such as an interaction between a CH_2 group and a CH_3 group. Between *like* UA (either CH_3 group or CH_2 group) interactions, the LJ potential parameters are listed in Table II. Additionally, between models A and B the bending potential[58] U_b is described by the Taylor series' *quadratic* term expansion of bending angle deviation and the torsion potential[58] U_t is expressed by a third-order *cosine* polynomial of a dihedral angle using the optimized potential for liquid simulations model[63] of Jorgensen *et al.* as shown in Eqs. (6) and (7), respectively,

$$U_b = \tfrac{1}{2}k_\theta(\theta_i - \theta_0)^2, \tag{6}$$

$$U_t = c_1(1 + \cos \phi_i) + c_2(1 - \cos 2\phi_i) + c_3(1 + \cos 3\phi_i). \tag{7}$$

B. Simulation methods

NEMD simulation contains two simulation systems: (1) constant volume NEMD or isochoric-isothermal NEMD (*NVT*-NEMD) (Refs. 10–12) and (2) constant pressure NEMD or isobaric-isothermal NEMD (*NPT*-NEMD) (Refs. 25–27, 30, 43, and 50) systems. The NEMD algorithm was originally developed by combining SLLOD equations of motion[10] of Edberg *et al.* with Lees–Edwards sliding brick periodic boundary condition.[64]

In general, the SLLOD algorithms involve two thermostatting schemes, namely, atomic and molecular center of mass versions. It has been shown by Edberg *et al.*[10] that the steady state responses to atomic and molecular shear are *equivalent* if the same (molecular) thermostat is used for both. In the absence of a thermostat, atomic and molecular shear only differ in that an initial delta function external force is applied to the centers of mass of all molecules for molecular shear, but applied to the individual atoms for atomic shear. The differences between the responses to

atomic and molecular center of mass shear decay as the steady state is approached.

The atomic stress tensor, including contributions from intermolecular and intramolecular force, is rigorously *symmetric* at all times. The *time averaged* atomic and molecular tensors should be *identical*; however, the molecular stress tensor may *not* be symmetric *instantaneously*. Significantly, for a system of rigid homonuclear *diatomic molecules* undergoing planar Couette flow, Travis *et al.*[65] have demonstrated that molecular stress tensor can contain a *nonvanishing antisymmetric* component due to body torques unintentionally applied by an atomic thermostat. In addition, enhanced *molecular alignment* is observed at high shear rates when an uncorrected atomic thermostat is employed. These problems can be corrected by applying an atomic thermostat so that the *molecular rotational degrees of freedom* are also properly thermostatted.

Further, the results of Travis *et al.*[65] show *shear thinning* for both the molecular and atomic thermostats, with a *dramatic drop* in viscosity for the atomic thermostatted fluid. This dramatic drop is due to the production of a *string phase*, i.e., an artificially induced, highly orientational ordered, low viscosity state. Additionally, both can obviously form the string phases in the shearing diatomic fluid if the velocity profile used to obtain the thermal velocities in the thermostat is assumed to remain linear at high shear rates. Eventually, the only practical way to avoid all of these problems for complex chain molecules is to keep the shear rate low enough so that the results of all thermostats agree. In the present study, we choose the atomic version including the equations of motion of SLLOD, temperature, and stress tensor to discuss liquid hexadecane molecules undergoing planar Couette flow.

This key algorithm is a particularly useful technique for studying rheological properties. SLLOD equations of motion can be implemented by the Leapfrog–Verlet scheme[66] of MacGowan and Heyes. For extremely high shear rates ($\geq 10^{12}$ s^{-1}), the magnitude of the time step was progressively decreased from 1.0 to 0.1 fs in order to ensure numerical stability. Equations of motion for both *NVT*-NEMD and *NVT*-NEMD algorithms, respectively, are described as follows.

1. NVT-NEMD algorithm

For a simulation system consisting of total number (N) atoms, equations of motion for *NVT*-NEMD simulation[10–12] are given by

$$\dot{\mathbf{q}}_i = \frac{\mathbf{p}_i}{m_i} + \dot{\gamma} y_i \mathbf{e}_x, \tag{8}$$

$$\dot{\mathbf{p}}_i = \mathbf{f}_i - \dot{\gamma} p_{yi}\mathbf{e}_x - \xi \mathbf{p}_i, \tag{9}$$

$$\xi = \frac{\sum_{i=1}^{N}(\mathbf{f}_i \cdot \mathbf{q}_i - \dot{\gamma} p_{xi} p_{yi})}{\sum_{i=1}^{N}\mathbf{p}_i^2}, \tag{10}$$

where $\mathbf{q}_i$ is the position vector of the ith atom, $\mathbf{p}_i$ is the peculiar momentum of the ith atom, y_i is a component of $\mathbf{q}_i$, p_{xi} and p_{yi} are a component of $\mathbf{p}_i$, m_i is the mass of the ith

atom, $\mathbf{f}_i$ is the interaction force on the ith atom, $\dot{\gamma}$ is the shear rate, $\mathbf{e}_x$ is a unit vector in the x direction, N equals the total number of atoms, and ξ is the Gaussian thermostat multiple.[11] In the momentum equation of motion of Eq. (9), the ξ parameter is applied to maintain the system in an isothermal state. The instantaneous system temperature is stabilized to the set temperature T_{set} by the *ad hoc* velocity rescaling method.[5,11] Specifically, the equations of motion for constant volume equilibrium molecular dynamics (NVT-EMD) system are obtained by setting $\dot{\gamma}=0$ in the equations above.

Furthermore, the various interaction forces on the ith atom $\mathbf{f}_i$ can be derived from the potential functions above by Hamiltonian's equation of motion[5]

$$\mathbf{f}_i = -\sum_{j\neq i}^{N} \nabla_i U(r_{ij}),\tag{11}$$

where $\mathbf{r}_{ij}$ denotes the distance vector from atom j to atom i. The derived results of LJ, stretching, bending, and torsion forces were briefly described in the study[67] of Chynoweth *et al.*

2. NPT-NEMD algorithm

Equations of motion of NPT-NEMD simulation[25–27,30,43,50] are shown below

$$\dot{\mathbf{q}}_i = \frac{\mathbf{p}_i}{m_i} + \dot{\gamma} y_i \mathbf{e}_x + \mathbf{q}_i \dot{\varepsilon},\tag{12}$$

$$\dot{\mathbf{p}}_i = \mathbf{f}_i - \dot{\gamma} p_{yi}\mathbf{e}_x - (\xi+\dot{\varepsilon})\mathbf{p}_i,\tag{13}$$

$$\dot{V} = 3V\dot{\varepsilon},\tag{14}$$

$$\ddot{\varepsilon} = \frac{(P - P_{\text{set}})V}{Q_p k_B T_{\text{set}}},\tag{15}$$

$$\xi = \frac{\sum_{i=1}^{N}(\mathbf{f}_i \cdot \mathbf{q}_i - \dot{\gamma} p_{xi} p_{yi})}{\sum_{i=1}^{N} \mathbf{p}_i^2} - \dot{\varepsilon},\tag{16}$$

where the system volume V and the Lagrange multiple ε are changed with the simulation time. In the momentum equation of motion of Eq. (13), the ε parameter can dominate the simulation system research to an isobaric state. As seen in Eq. (16), the Gaussian thermostat multiple ξ is affected by the Lagrange multiple.[25] T_{set} and P_{set} are the set values of the system temperature and pressure, respectively. Q_p is a damping constant and k_B is Boltzmann's constant (1.381×10^{-23} J/K).

Naturally, NPT-NEMD simulation at $\dot{\gamma}=0$ corresponds to NPT-EMD (constant pressure equilibrium molecular dynamics) simulation. Notably, Q_p is a factor chosen by the trial and error method[25] to give a good damping of pressure fluctuations. This factor indirectly affects the stability to predict volume, as seen in Eqs. (14) and (15). In this study, $Q_p = 100/k_B T_{\text{set}}$.

To obtain an effective stable numerical solution of the volume equation, the modified pressure method[50] of Wang and Fichthorn was used. The volume equation corresponded

to a three-dimensional variation of the system volume, where the geometry of the system volume used in this study was a rectangle. As the sizes of flow and gradient directions were held constant during simulation, the variation of the system volume is determined by the size of the periodic boundary conditional direction. In Sec. III C, this conclusive test method is simply explained and can be further applied in NPT-NEMD system.

C. Statistical properties

Stress tensor is an important statistical property in the area of MD simulation. In this study, thermodynamic states including temperature and pressure and rheological properties of viscosity are the primary measured values used to analyze the steady state simple shear flow system.

1. Temperature and pressure

The temperature[5] of an atomic system at equilibrium is related to the kinetic energy of the system's atoms in which,

$$T = \frac{1}{3Nk_B}\sum_{i=1}^{N}\frac{\mathbf{p}_i^2}{m_i}.\tag{17}$$

For a homogenous atomic system at equilibrium, the stress tensor is given by the Irving–Kirkwood equation[5,31,68]

$$\tau_{\alpha\beta} = -\frac{1}{V}\left(\sum_{i=1}^{N}\frac{p_{i\alpha}p_{i\beta}}{m_i} + \sum_{i=1}^{N}\sum_{j>i}^{N} r_{ij\alpha}f_{ij\beta}\right),\tag{18}$$

where $\tau_{\alpha\beta}$ is a component of the stress tensor; subindices $\alpha,\beta=x,y,z$; and f_{ij} denotes the force exerted on the atom i due to atom j. In the stress tensor equation, the *first* sum on the right side of Eq. (18) describes the contribution of the kinetic energy, and the *second* sum describes the contribution of virial energy. The force term f_{ij} consists of both LJ and bonding interactions, which contain the bond stretching, bond bending, and torsion potentials. The expressions of these forces' virial energy were briefly defined in the stress tensor study[69] of Carpenter.

Furthermore, the atomic hydrostatic pressure[31] is given by negative one-third of the trace of the stress tensor,

$$P = -\tfrac{1}{3}(\tau_{xx} + \tau_{yy} + \tau_{zz}).\tag{19}$$

Note that the bond bending and torsion interactions do not contribute to the pressure.[69]

2. Viscosity

For a NEMD system, the viscosity[31] in the simple shear flow field is defined by

$$\eta(\dot{\gamma}) = \frac{\tau_{yx}}{\dot{\gamma}},\tag{20}$$

where τ_{yx} is the yx component of the stress tensor, and $\eta(\dot{\gamma})$ indicates the shear rate dependence of shear thinning viscosity. As the shear rate approaches zero, all fluids exhibit Newtonian behavior, which allows the determination of the zero-shear-rate viscosity η_0, i.e., $\eta_0 = \lim_{\dot{\gamma}\to 0}\eta(\dot{\gamma})$.

TABLE III. Comparison of heat of vaporization of *n*-hexadecane for both potential models A and B with the previous predicted values of Chynoweth and Michopoulos and experimental data.

State points		Heat of vaporization ΔH_v (kJ/mol)			
T (K)	ρ (g/cm^3)	Expt.[a]	Model A (previous study[b])	Model A (present study)	Model B (present study)
298	0.770	81.17	76.99	77.91	87.44
560	0.572	51.04	52.72	53.61	59.23

[a]Taken from Refs. 19 and 71.
[b]Taken from Ref. 19.

III. RESULTS AND DISCUSSION

Liquid *n*-hexadecane fluid is analyzed in this study. First, in Secs. III A and III B, we present the comparison results between two different potential models on the fluids of thermodynamic and rheological properties. Then, in Sec. III C, we verify the agreement of constant pressure nonequilibrium molecular dynamics (*NPT*-NEMD) simulation with constant volume nonequilibrium molecular dynamics (*NVT*-NEMD) simulation. Next, in Sec. III D, we analyze how thermodynamic states of *P-V-T* data are influenced by exerted shear rates and the variation of shear dilatancy at high shear rates. Lastly, from a rheological perspective, Sec. III E explores the influence of pressure and temperature on shear thinning using *NPT*-NEMD simulation. Also, in *NVT*-NEMD simulation we comprehend the change in shear thinning at various densities.

A. Thermodynamic properties

Understanding thermodynamic properties, such as heat of vaporization and liquid-vapor coexistence curve, of materials in the liquid state is important. In this section, calculated thermodynamic properties using two different potential models are compared quantitatively with the related experimental results.

1. Heat of vaporization

The heat, or enthalpy, of vaporization ΔH_v is the enthalpy change that occurs during the transition of a substance from the liquid to the gas phase. Under the assumption that the gas is *ideal* and that the kinetic energies in the gas and liquid phases are identical at a constant temperature, ΔH_v can be approximated as follows:[70]

$$\Delta H_v(T) = H_{\text{gas}} - H_{\text{liquid}} \approx RT - [U_{\text{liquid}}(\text{inter}) + PV_{\text{liquid}}],$$

$$(21)$$

where H_{gas} and H_{liquid} are the enthalpy of the gas and liquid phases, respectively; R is the gas constant (8.314 J/mol K); and $U_{\text{liquid}}(\text{inter})$ is the intermolecular potential in the liquid phase, namely, vdW interaction between different molecular chains. The heat of vaporization equation of Eq. (21) was derived[70] by Horn *et al.*, who predicted ΔH_v of water molecules by using *NPT*-EMD (constant pressure equilibrium molecular dynamics) simulation, which approximated values obtained experimentally. Therefore, we further utilized their equation to calculate ΔH_v of *n*-hexadecane molecules.

The ΔH_v values were estimated via Eq. (21) for liquid and gas *n*-hexadecane under the standard condition ($T = 298$ K and $\rho = 0.770$ g/cm^3) and at the boiling point ($T = 560$ K and $\rho = 0.572$ g/cm^3), which will be referred to as state points 1 and 2, respectively. A cubic box, with three-dimensional periodic boundary conditions containing 144 *n*-hexadecane molecules was used in *NVT*-EMD (constant volume equilibrium molecular dynamics) simulation. The time step used to integrate the equations of motion was 2.0 fs, and the total simulation time was set 1000.0 ps. Potential models A and B were used to estimate ΔH_v.

In the present study the variation of ΔH_v at two state points rapidly converged to a stable condition for two different potential models. The predicted ΔH_v using *NVT*-EMD simulation from both previous predicted[19] values and results of the present study are shown together in Table III alongside experimental data.[19,71]

In each case, values for ΔH_v using model B are higher than model A. Looking at the same potential model A and state points in Table III, our simulation results closely approached the predicted ΔH_v values[19] of Chynoweth and Michopoulos. Furthermore, ΔH_v values using model A is roughly close to their corresponding experimental values,[19,71] with less than 4%–7% derivation. In contrast, the difference between the ΔH_v value of model B and the experimental data is slightly larger.

As seen in Eq. (21), ΔH_v contains three parts: the system temperature term TR, the pressure-volume term PV, and the intermolecular potential $U_{\text{liquid}}(\text{inter})$. In this study, $U_{\text{liquid}}(\text{inter})$ was the main contributor to ΔH_v and made up about 93% of the total value. As the LJ potential depends on $U_{\text{liquid}}(\text{inter})$, it is understood that the different LJ potential parameters of Table II directly affect the predicted values of ΔH_v. Therefore we have suggested that potential model A possesses the ability to predict the heat of vaporization better than potential model B.

2. Liquid-vapor coexistence curve

The phase of a substance is sensitive to changes in temperature and density. Here, variations of the liquid-vapor coexistence curve of *n*-hexadecane molecules were studied via *NVT*-EMD simulation using potential models A and B.

The volume of the simulation box was $V = L_x \times L_y \times L_z$ with $L_x = 4.0$ nm, $L_y = 4.0$ nm, and $L_z = 12.5$ nm, where L_x, L_y, and L_z are *x*, *y*, and *z* directional sizes, respectively. The box contained 240 *n*-hexadecane molecules with three-dimensional periodic boundary conditions. The time step was
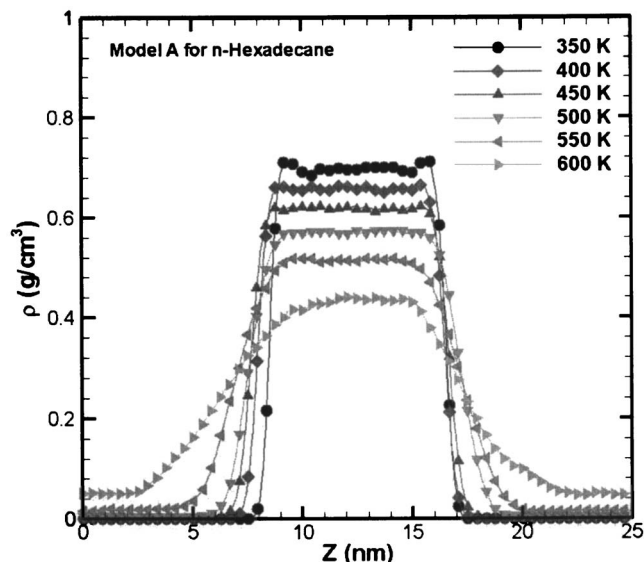
FIG. 2. *Z*-directional density profiles of *n*-hexadecane at coexistence in a temperature range of 350–600 K as obtained by *NVT*-EMD simulation using the potential model A.

FIG. 3. *Z*-directional density profiles of *n*-hexadecane at coexistence in a temperature range of 350–650 K as obtained by *NVT*-EMD simulation using the potential model B.

set at 2.0 fs. The simulation system reached equilibrium and took the form of a fluid block during a total simulation time of 1.0 ns. In the following simulation, the *z*-directional length L_z of the box was extended to 25.0 nm, i.e., twice the original *z*-directional size. Once the fluid expanded to fill the larger system volume, the fluid block gradually converged to a new equilibrium state during total *NVT*-EMD simulation time of 1.0 ns, again. This extended system reached the liquid-vapor phase at its equilibrium state. Thus, the *z*-directional density profile showed two symmetric interfaces of the hyperbolic tangent function, which indicates the existence fluid with both liquid and vapor densities.

The fluid's *z*-directional density profile was predicted at various temperatures using potential models A and B. The results are shown in Figs. 2 and 3. Over the range of temperatures in the simulation, two symmetric interfaces containing liquid and vapor phases appeared in the density profiles, as shown below. The plateau and lowland regions present the existence of liquid and vapor densities, respectively. Over the temperature range of 350–400 K, the density profiles show complete liquid phases and contain no gas molecules. As the temperature increased to 450 K, a few gas molecules appear. Until temperatures over 500 K, the density profiles started to clearly show the curve of both liquid and vapor phases.

The liquid and vapor densities for models A and B can be extracted in Figs. 2 and 3. As shown by the liquid-vapor coexistence curves of Fig. 4, the liquid density of model B is apparently higher than model A, and correspondingly the vapor density of model B is lower than model A. When using the same potential model B, our liquid-vapor coexistence curve is in excellent agreement with the results of López-Lemus *et al.*[59] and is also near to the related experimental curve;[59,72] however, the difference between the liquid-vapor density of model A and the experimental data is larger. Moreover, for model B, the critical point of *n*-hexadecane molecules can be found via the law of rectilinear diameters and
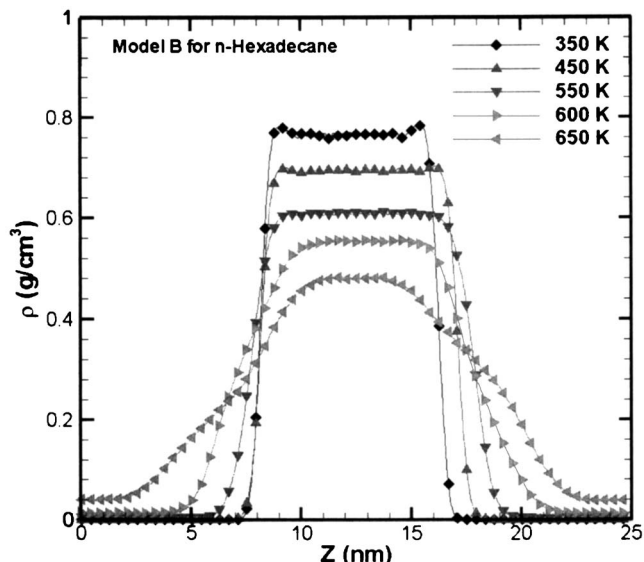
Ising's scaling law[73,74] by fitting the liquid-vapor coexistence data to obtain the critical density and temperature as follows:

$$\frac{\rho_l + \rho_v}{2} = \rho_c + C_1(T - T_c), \quad (22)$$

$$\rho_l - \rho_v = C_2(T - T_c)^\beta, \quad (23)$$

where ρ_l and ρ_v are the liquid and vapor densities, respectively; ρ_c and T_c are the critical density and temperature; β is the Ising-type critical exponent[73] of 0.32; and C_1 and C_2 are the fitting parameters.

Finally, our estimated critical point of 720.9 K and 0.235 g/cm³ was in close agreement with experimental data[60,75] at 723.6 K and 0.219 g/cm³. Between different po-
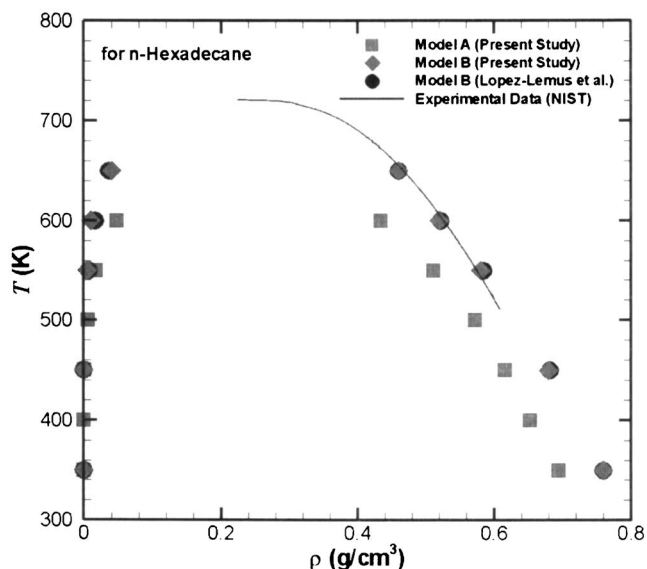

FIG. 4. Liquid-vapor coexistence curves of *n*-hexadecane for both potential models A and B compared with the previous predicted values of López-Lemus *et al.* (Ref. 59) and experimental data (Refs. 59 and 72).
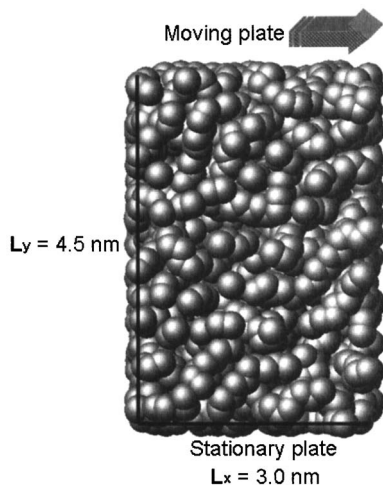
FIG. 5. Dimensions of simulation box for planar shear flow system of liquid *n*-hexadecane between a moving upper plate and a stationary lower plate: (a) L_x=3.0 nm in the flow direction (*x* axis) and (b) L_y=4.5 nm in the gradient direction (*y* axis).

FIG. 6. Shear rate $\dot{\gamma}$ dependence on viscosity η of *n*-hexadecane at a state point of 477.6 K and 0.896 g/cm³ for both potential models A and B as obtained from *NVT*-NEMD simulation compared with the predicted values of Chynoweth *et al.* (Ref. [20]). Solid (dashed) lines correspond to curves fitted to η-$\dot{\gamma}$ simulation data using the Cross model (power law). Arrows above indicate critical shear rates.

tential models A and B, the predictions of the liquid-vapor coexistence curve fit well, qualitatively. Correspondingly, the quantitative description of the liquid-vapor coexistence curve via model B is in better agreement with experimental data than via model A. So far, the above results firmly support the validity of *NVT*-EMD simulations program in the present study.

B. Rheological properties

When analyzing the rheology of fluids, the viscosity is an important fluid property, because it represents a material's internal resistance to deform. For a non-Newtonian fluid the viscosity–shear rate relationship (η-$\dot{\gamma}$) contains two components, namely, the Newtonian fluid regime's zero-shear-rate viscosity and the non-Newtonian fluid regime's shear thinning behavior. Additionally, by using the inverse of the Rouse model rotational relaxation time,[13,25,46,76] the critical shear rate indicates that the transition from Newtonian to non-Newtonian behavior is observable.[13,25]

Here, we discuss the rheological properties in *NVT*-NEMD simulation for different potential models. As the simulation system shown in Fig. 5, a rectangular three-dimensional box with L_x=3.0 nm, L_y=4.5 nm, L_z=4.5 nm and containing 144 *n*-hexadecane molecules at a state point of 477.6 K and 0.896 g/cm³ was used. The *x*, *y*, and *z* directions of the system box correspond to flow, gradient, and periodic boundary condition directions, respectively. The simulation was run over a wide range of shear rates, $1 \times 10^{8.5}$–$1 \times 10^{12.5}$ s⁻¹. The analysis is divided into two parts to discuss rheological properties for both different potential models A and B below.

1. Shear thinning behavior and zero-shear-rate viscosity

We plotted a conventional η-$\dot{\gamma}$ flow curve, namely, the traditional log η versus log $\dot{\gamma}$ data. In Fig. 6, the observed reduction in viscosity with increasing shear rate is known as shear thinning behavior, which is a clear manifestation of the
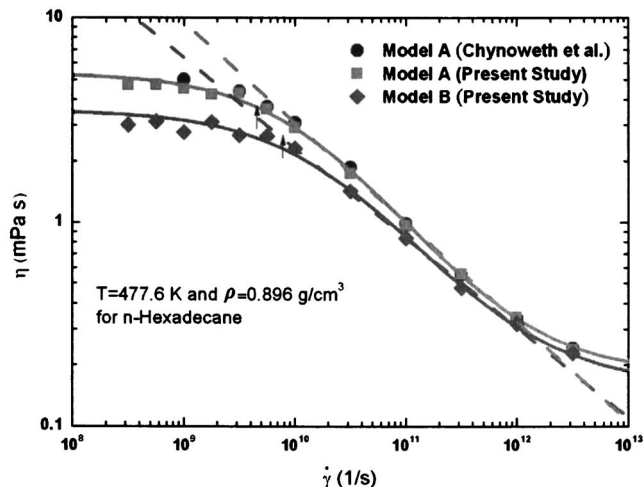
non-Newtonian nature of the fluid. The linear behavior of the log η versus log $\dot{\gamma}$ data in the shear rate region of $1 \times 10^{10.0}$–$1 \times 10^{12.0}$ s⁻¹ presents a "power law" relationship[19,48] of shear rates,

$$\eta(\dot{\gamma}, A_k, k) = A_k \dot{\gamma}^k, \quad 1 \times 10^{10.0} \text{ s}^{-1} \leqslant \dot{\gamma} \leqslant \times 10^{12.0} \text{ s}^{-1},$$

(24)

where A_k is a constant of proportionality, and *k* is the power law exponent. As seen in Fig. 6, a power law curve was fitted to the data and is indicated by the dashed lines. In both models A and B the exponents are −0.472 and −0.438, respectively, which fall reasonably within the range of −0.4 to −0.9 often reported[47] for liquid polymers.

As found in the lower shear rate region of $\dot{\gamma} < 1 \times 10^{9.0}$ s⁻¹, the Newtonian plateau regime's zero-shear-rate viscosity follows the non-Newtonian fluid regime's shear thinning behavior. It was found that the extrapolated[8,20] zero-shear-rate viscosity η_0, shown in Fig. 6, can be found via the Cross model[8,20,48] by fitting the log η versus log $\dot{\gamma}$ data,

$$\eta(\dot{\gamma}; \eta_0; \eta_\infty; \lambda, n_s) = \eta_\infty + \frac{\eta_0 - \eta_\infty}{1 + (\lambda \dot{\gamma})^{n_s}}.$$

(25)

The Cross model has four parameters: η_0 is the very low shear rate viscosity, or zero-shear-rate viscosity; η_∞ is the very high shear rate viscosity; λ is the dimensions of time; and n_s is the dimensionless exponent, which controls the slope in the shear thinning region. In Fig. 6, solid lines represent curves fit via the Cross model. In potential model A, η_0=5.39 mPa s, η_∞=0.18 mPa s, n_s=0.79, and λ=87.89 ps. In potential model B, η_0=3.55 mPa s, η_∞=0.16 mPa s, n_s=0.75, and λ=61.64 ps.

Referring to the same state point (477.6 K and 0.896 g/cm³) in potential model A, our predicted η-$\dot{\gamma}$ flow curve are in excellent agreement with the results[20] of Chynoweth *et al.* When comparing potential models A and B, the η_0 value of model A is higher than that of model B;

TABLE IV. Various rheological properties of n-hexadecane for both potential models A and B at a state point of 477.6 K and 0.896 g/cm^3. (Experimental data taken from Refs. [20] and [71] of zero-shear-rate viscosity at 8.34 mPa s.)

	Model A	Model B
k	−0.472	−0.438
η_0 (mPa s)	5.392	3.551
τ (ps)	208.2	137.1
$\dot{\gamma}_e$ (s^{-1})	4.8×10^9	7.3×10^9

however, both models agree closely with respect to n_s and η_∞. Experimentally, at a state point of 477.6 K and 0.896 g/cm^3, η_0 is 8.34 mPa s. Model A's η_0 value of 5.39 mPa s is in close agreement with experimental value[20,71] better than model B's η_0 value of 3.55 mPa s. In summary, when different potential models A and B are compared, the predictions of the η-$\dot{\gamma}$ flow curve fit well qualitatively. In contrast, the quantitative prediction of η_0 via model A is in close agreement with experimental data than those of model B. Consequently, in the present study, the results above strongly support the validity of NVT-NEMD simulation program for predicting the shear thinning relationship between viscosity and shear rate.

2. Rotational relaxation time and critical shear rate

The rotational relaxation time is the characteristic time of polymer chain relaxation. For a polymer chain, n-hexadecane is considered a short molecular chain; therefore, the rotational relaxation time[13,25,46,76] of n-hexadecane can be determined by the Rouse model

$$\tau_R = \frac{6\eta_0 M}{\pi^2 \rho R T}, \tag{26}$$

where τ_R is the rotational relaxation time, M is the molecular weight, and ρ is the equilibrium density.

The critical shear rate γ_c indicates the starting point of shear thinning, or the transition from Newtonian to non-Newtonian behavior. Berker $et\ al.$[13] found that $\gamma_c = \tau_R^{-1}$, which is in approximate agreement with the observed NEMD simulation data.

As seen in Table IV, the rotational relaxation time and critical shear rate are calculated by extrapolating the zero-shear-rate viscosity η_0 and the Rouse model of Eq. (26). τ_R values of models A and B are 208.2 and 137.1 ps, respectively. In addition, γ_c values of model A and B (4.8×10^9 and 7.3×10^9 s^{-1}) are marked by arrows in the η-$\dot{\gamma}$ flow curve of Fig. 6, respectively. Obviously, the critical shear rate is shown to be the transition point from Newtonian to non-

Newtonian regimes. As a consequence, the values of γ_c for models A and B are in close agreement with observed NEMD simulation data.

As the analyses of Secs. III A and III B above demonstrate, the qualitative description of n-hexadecane using MD simulation nearly matches the actual physical behavior for each potential model studied. Therefore, potential model A has the ability to predict rheological properties of the zero-shear-rate viscosity, while potential model B has the ability to predict thermodynamic properties of the liquid-vapor coexistence curve. In the following section, we further expand our discussions with respect to rheological properties via potential model A.

C. Agreement between NVT-NEMD and NPT-NEMD simulations

Previously, under hypothesis of a constant density condition, the configurative variation in the x, y, and z sizes of the system box affecting the fluid's statistical properties were $unknown$. In the following section, we will examine simply the aforementioned problem. Further, this undertaking has the additional benefit of further demonstrating the agreement between NPT-NEMD and NVT-NEMD simulations under both constant temperature and shear rate conditions.

1. Adjusted density of NVT-NEMD simulation

In the next discussions in Secs. III D and III E, the density of the fluid is varied by adjusting the dimensions of the system box. As the results show, the simulation provides reliable results regardless of the system box configuration. As seen in Fig. 5, the system box was not cubic, with three dimensions of $3.0 \times 4.5 \times 4.5$ nm^3. The system contained liquid 144 n-hexadecane molecules with an initial density of 0.896 g/cm^3. As the system density was abruptly reduced from 0.896 to 0.842 g/cm^3, the three directional sizes of the system were varied in the directions of flow, gradient, and periodic boundary condition. In each simulation, one of three directional sizes was changed while the other two were held constant. Three different configurative dimensions of the simulation box are shown in Table V. The NVT-NEMD simulations were performed at 477.6 K and $1 \times 10^{12.0}$ s^{-1} during 1000.0 ps. By choosing a high shear rate of $\dot{\gamma} = 1 \times 10^{12.0}$ s^{-1} the statistical properties in the shear flow system converged quickly due to rapid initial gains.

In the NVT-NEMD system at the same density of 0.842 g/cm^3 for different configurations of simulation box's dimensions, the convergent data of pressure and viscosity variation with simulation time are arranged in Table V. Initially, three respective cases of the system box configurations in the variation of pressure and viscosity do not match pretty

TABLE V. Simulation box dimensions (L_x, L_y, L_z), the convergent data of pressure P, and viscosity η as density is changed from 0.896 ($V = 3.0 \times 4.5 \times 4.5$ nm^3) to 0.842 g/cm^3 with 144 n-hexadecane molecules.

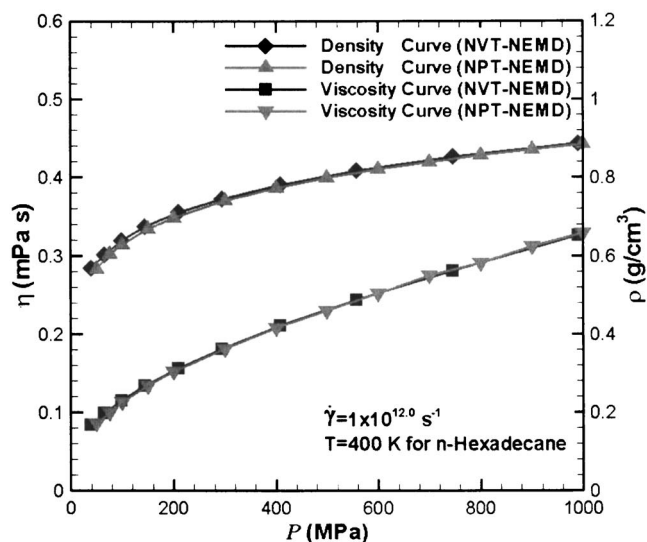|	Lx (nm)	L_y (nm)	L_z (nm)	P (MPa)	η (MPa s)
Flow direction	2.8	4.5	4.5	848.4	0.2844
Gradient direction	3.0	4.2	4.5	848.2	0.2840
Periodic direction	3.0	4.5	4.2	848.1	0.2836

FIG. 7. Pressure P dependence of density ρ and viscosity η for n-hexadecane at 400 K and 1×10^{12} s^{-1} obtained from NVT-NEMD and NPT-NEMD simulations.

well; however, the pressure and viscosity for all cases finally converged to about 848 MPa and 0.284 mPa s as the simulation progressed. The viscosity study[20] of Chynoweth *et al.*, performed using the same potential model A at the same condition of 477.6 K, 0.842 g/cm^3, and $1 \times 10^{12.0}$ s^{-1}, resulted in a viscosity of 0.285 ± 0.004 mPa s. As our calculated value reasonably falls within their results for the viscosity, the simulation is shown to be reliable. Furthermore, the results at the same density show that the variations in the dimensions of the simulation box do not affect surely the convergence of statistical properties.

2. Validity of NPT-NEMD simulation

As discussed above in Sec. II B 2, volume differential equation in Eq. (14) corresponds to the variation of the three directional dimensions of the simulation box. When the flow and gradient directional sizes are held constant, the magnitude of the adjusted volume corresponds to the change in the *periodic boundary condition* (PBC). By selecting the PBC size, the algorithm of the simulation program does not require substantive modifications. From the previous section, we have known that adjusting the constituent dimensions of the simulation box do not affect the convergence of the fluid's statistical properties. Hence, adjusting the PBC size is an optimum choice in this study.

Under both constant temperature and shear rate (400 K and $1 \times 10^{12.0}$ s^{-1}) conditions, the agreement between NPT-NEMD and NVT-NEMD simulations is proved for a simulation system containing 144 n-hexadecane molecules. The flow and gradient directional sizes of simulation box are held constant at $L_x = 3.0$ nm and $L_y = 4.5$ nm, respectively. In NPT-NEMD simulation, the temperature value was 400 K and the pressure ranged from 50 to 1000 MPa. In NVT-NEMD simulation, the temperature value was also 400 K and the density ranged from 0.566 to 0.886 g/cm^3. Figure 7 shows the density-pressure and viscosity-pressure relationships. Expectably, the results show that density and

viscosity increase with pressure. This result is consistent with the general physical understanding. Clearly, both NPT-NEMD and NVT-NEMD curves overlay closely for each data point, suggesting near agreement between NPT-NEMD and NVT-NEMD simulations. Obviously, such result supports the validity of NPT-NEMD simulation program in this study.

D. Variations of shear dilatancy

As this study focuses on nonequilibrium thermodynamic problems, we extend the space of thermodynamic variables, which consists of pressure (P), temperature (T), density (ρ)/volume (V), and shear rate ($\dot{\gamma}$), to understand how shear rate affects P-ρ-T data. In addition, using P-ρ-T data and Doolittle's free volume concept is helpful in analyzing the variations of viscosity as shown in the next section of Sec. III E.

At high shear rates, shear dilatancy[22] exhibits nonlinear behavior in nonequilibrium thermodynamic states. As occurred in NVT-NEMD (Refs. 22–24, 28, and 29) system, shear dilatancy presents shear rate's dependence on pressure. Correspondingly, as occurred in NPT-NEMD (Refs. 19, 22, 25–27, and 30) system, shear dilatancy presents shear rate's dependence on density.

The geometry and dimensions of the simple shear flow are illustrated in Fig. 5. The simulation box, containing 144 n-hexadecane molecules, is rectangular with flow and gradient directional sizes of $L_x = 3.0$ nm and $L_y = 4.5$ nm, respectively. The periodic boundary condition is applied in the z direction of the system. Over a wide shear rate range between $1 \times 10^{9.0}$ and $1 \times 10^{12.5}$ s^{-1}, the change in nonequilibrium thermodynamic states is observed. Shear dilatancy in NPT-NEMD simulation is influenced by both temperature and pressure effects. At different densities, the change in shear dilatancy is also analyzed using NVT-NEMD simulation.

1. Temperature effect

Using NPT-NEMD simulation of liquid n-hexadecane at a constant pressure of 250 MPa in a temperature range between 300 and 500 K, it is understood that the density-temperature (ρ-T) relationship is influenced by different shear rates of $1 \times 10^{9.5}$–$1 \times 10^{12.5}$ s^{-1}. In this study, the wide shear rate range spans three orders of magnitude from higher rate of $1 \times 10^{12.5}$ s^{-1} to lower rate of $1 \times 10^{9.5}$ s^{-1}. Figure 8 shows one equilibrium state curve and six nonequilibrium state curves at different shear rates in the ρ-T relationship, where the equilibrium state curve can be obtained from NPT-NEMD simulation set at zero-shear rate, namely, $\dot{\gamma} = 0$. From the figure, a decrease in density with increasing temperature is clearly seen. In a higher shear rate range of $1 \times 10^{11.5}$–$1 \times 10^{12.5}$ s^{-1}, the density decreases with increasing shear rate. However, as the shear rate decreases to 1×10^{11} s^{-1} the nonequilibrium state curve closely approximates the equilibrium curve. Similarly, at the lowest shear rates of $1 \times 10^{9.5}$ and 1×10^{10} s^{-1}, both state curves closely approach the equilibrium curve, although, the nonequilib-
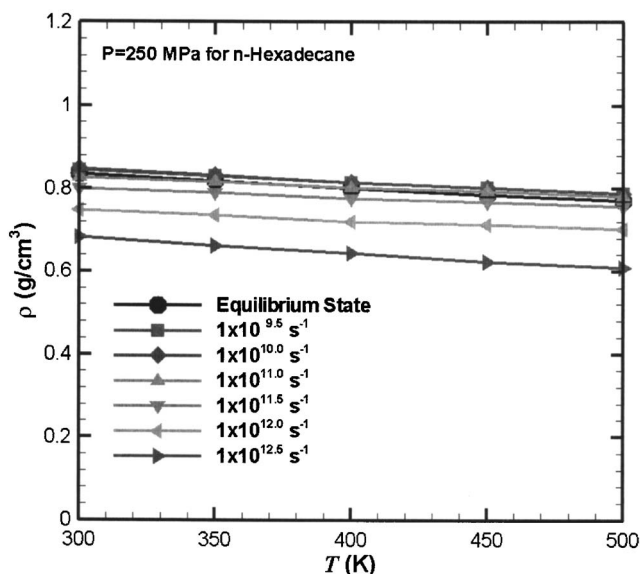
FIG. 8. Temperature T dependence of density ρ for n-hexadecane at 250 MPa and shear rates between $1 \times 10^{9.5}$ and $1 \times 10^{12.5}$ s^{-1} obtained by *NPT*-NEMD simulation and compared with equilibrium state data.

rium state curves are slightly higher than the equilibrium curve due to thermonoise, which produces the statistical errors.

As shown in Fig. 9, analysis of the density–shear rate $(\rho\text{-}\dot{\gamma})$ curves are at five different temperature of 300, 350, 400, 450, and 500 K. Specifically, at $\dot{\gamma} < 1 \times 10^{11}$ s^{-1} the density remains constant and is approximately equal to the equilibrium density $[\rho(\dot{\gamma}) \approx \rho(\dot{\gamma}=0)]$. This result suggests that the shear rate is independent of density for these values, namely, the fluid behaves like the Newtonian fluid regime. Conversely, at $\dot{\gamma} > 1 \times 10^{11}$ s^{-1} the density rapidly decreases with increasing shear rate. This $\rho\text{-}\dot{\gamma}$ relationship at high shear rates is known as *shear dilatancy*. Comparably, the density variation induced by shear rate in Fig. 9 is consistent with the result in Fig. 8. To quantify shear dilatancy behavior in constant pressure NEMD simulation, Xu et al.[27] suggested that shear dilatancy's $\rho\text{-}\dot{\gamma}$ curve can be described by the power law
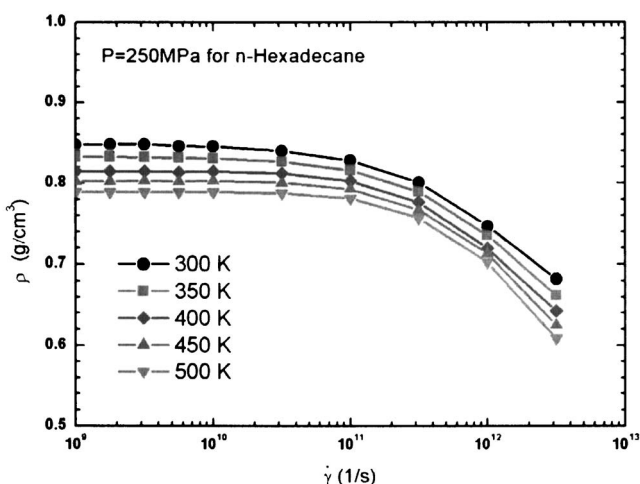

FIG. 9. Shear rate $\dot{\gamma}$ dependence of density ρ for n-hexadecane at 250 MPa and various temperatures obtained by *NPT*-NEMD simulation.
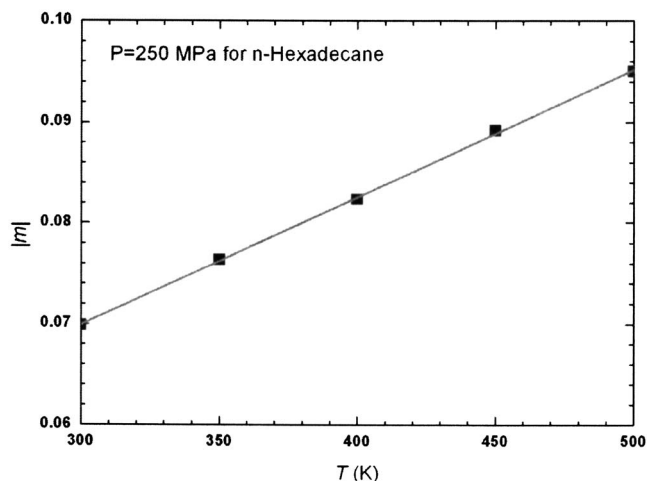

FIG. 10. The absolute value of the power law's exponent $|m|$ vs temperature T illustrates the dependence of density on shear rate for n-hexadecane at 250 MPa and shear rates of over $1 \times 10^{11.0}$ s^{-1}. The line is a linear curve fit to the data.

$$\rho(\dot{\gamma}, A_m, m) = A_m \dot{\gamma}^m, \quad \dot{\gamma} > 1 \times 10^{11.0} \text{ s}^{-1}, \quad (27)$$

where A_m is a constant of proportionality, and m is the power law's exponent. In general, the exponent m is a *negative* value for alkane molecules in many studies,[19,22,25–27,30] which is presented by a decrease in density with an increase in shear rate. Specifically, in the results of Xu et al.,[27] the density increased with an increase in shear rate for long molecular chains of 30 FENE beads. In addition, earlier research using *NPT*-NEMD simulation for Ar gases, Hood et al.[22] suggested that at a triple point the power law's exponent of shear dilatancy equals 3/2, i.e., $\rho \propto \dot{\gamma}^{3/2}$.

Furthermore, the $\rho\text{-}\dot{\gamma}$ data at $\dot{\gamma} > 1 \times 10^{11.0}$ s^{-1} in Fig. 9 were fitted by the power law to gain an exponent m. Figure 10 shows the temperature dependence of the absolute value of the power law's exponent $|m|$. The $|m|$ value is relative to the degree of shear dilatancy, given by the absolute slope of the $\rho\text{-}\dot{\gamma}$ curve in constant pressure NEMD simulation under $\dot{\gamma} > 1 \times 10^{11.0}$ s^{-1} condition. As a result, the $|m|$ variation illustrated that the degree of shear dilatancy linearly increased with temperature, as shown in Fig. 10, which highlights the effects of the temperature on shear dilatancy.

2. Pressure effect

Using *NPT*-NEMD simulation of liquid n-hexadecane at a constant temperature of 400 K over a wide pressure region between 50 and 1000 MPa, the influence of varying shear rates on the density-pressure $(\rho-P)$ relationship can be understood. Figure 11 shows one equilibrium state curve and six nonequilibrium state curves at different shear rates in the $\rho-P$ relationship. Setting $\dot{\gamma}=0$, we can obtain the equilibrium state curve. From the figure, the density increases with an increase in pressure; however, at higher shear rates of over 1×10^{11} s^{-1}, the density decreased with an increase in shear rate. Specifically, as the shear rate falls to 1×10^{11} s^{-1} the slope of the nonequilibrium state's curve approaches the slope of the equilibrium state's curve. At lower shear rates of $1 \times 10^{9.5}$ and 1×10^{10} s^{-1}, both state's curves also match closely, although the nonequilibrium state curves
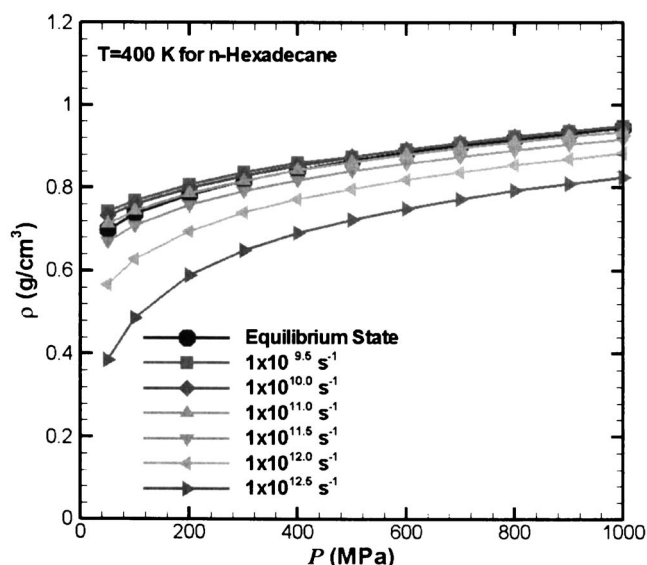
FIG. 11. Pressure P dependence of density ρ for n-hexadecane at 400 K and shear rates between $1 \times 10^{9.5}$ and $1 \times 10^{12.5}$ s^{-1} obtained by NPT-NEMD simulation and compared with equilibrium state data.

are somewhat higher than the equilibrium state's curve. Overall, the density variation induced by shear rate in Fig. 11 is also consistent with the results in Fig. 8.

As seen in Fig. 12, the density-shear rate (ρ-$\dot{\gamma}$) curves are at six different pressures of 50, 100, 250, 500, 750, and 1000 MPa. Clearly, the figure indicates that the density increases with increasing pressure. At $\dot{\gamma} < 1 \times 10^{11}$ s^{-1}, the density closely remains constant indicating that the density is independent of shear rate at these values. Also, these nonequilibrium state densities are approximately equal to the equilibrium density, namely, $\rho(\dot{\gamma}) \approx \rho(\dot{\gamma}=0)$ signifies that the liquid is very near its Newtonian fluid regime. In contrast, at $\dot{\gamma} > 1 \times 10^{11}$ s^{-1}, shear dilatancy is seen as the density decreased with an increase in shear rate. In the lower pressure region of 50 and 100 MPa, the density *rapidly* decreased with increasing shear rate; however, in the higher pressure region of 500, 750, and 1000 MPa, the density *slowly* decreased with increasing shear rate.
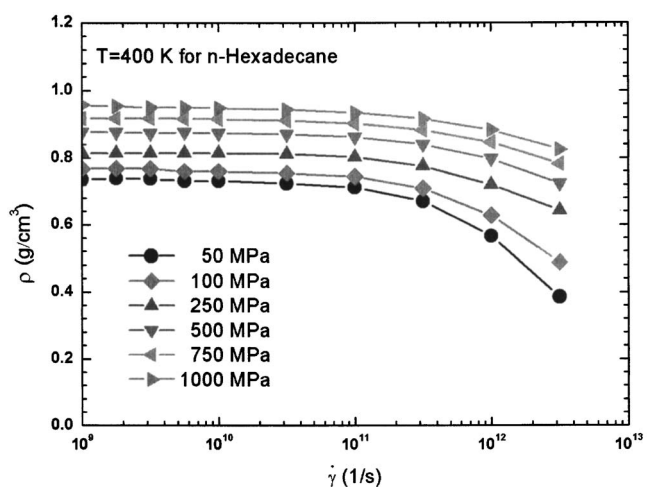

FIG. 12. Shear rate $\dot{\gamma}$ dependence of density ρ for n-hexadecane at 400 K and varying pressures obtained by NPT-NEMD simulation.
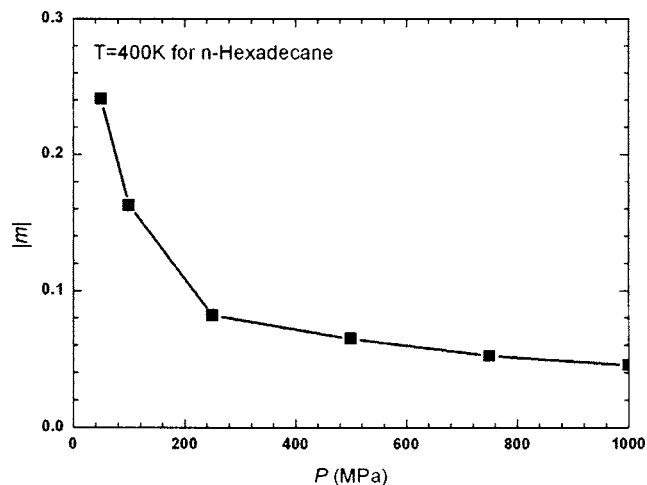

FIG. 13. The absolute value of the power law's exponent $|m|$ vs pressure P illustrates the dependence of density on shear rate for n-hexadecane at 400 K and shear rates of over $1 \times 10^{11.0}$ s^{-1}.

Again, the ρ-$\dot{\gamma}$ data at $\dot{\gamma} > 1 \times 10^{11.0}$ s^{-1} in Fig. 12 is fitted by the power law[27] to gain the exponent m. Note that $|m|$ represents the degree of shear dilatancy. Figure 13 shows the $|m|$ versus P relationship on shear dilatancy using NPT-NEMD simulation. As revealed in the figure, a turning point exists between 100 and 250 MPa. The $|m|$ value rapidly decreased with increased pressure before reaching the turning point. Correspondingly, the slope change in $|m|$ with increasing pressure slowly decreased after reaching the turning point. At high pressure regions of over 1000 MPa this slope should continue to decrease and approach a nearly constant value. In other words, the change in shear dilatancy is quite sensitive at lower pressures; however, the change is gradual at higher pressures.

Comparatively, we analyze that changes in pressure and temperature have opposing influence on NPT-NEMD simulation's shear dilatancy. Referring back to the discussion presented in Figs. 10 and 13, the findings present an increase in pressure reducing the degree of shear dilatancy and an increase in temperature increasing the degree of shear dilatancy.

3. Density effect

Using NVT-NEMD simulation of liquid n-hexadecane at a constant temperature of 400 K in a shear range of $1 \times 10^{9.5}$–$1 \times 10^{12.5}$ s^{-1}, we understand that the pressure-shear rate relationship (P-$\dot{\gamma}$) is influenced by different densities of 0.70, 0.75, 0.80, 0.85, and 0.90 g/cm^3. As seen in Fig. 14, P-$\dot{\gamma}$ indicates that the pressure increases with increasing density. At lower shear rates of $\dot{\gamma} < 1 \times 10^{11}$ s^{-1} the pressure remains relatively constant, indicating that shear rate is independent of pressure at lower shear rates, namely, $P(\dot{\gamma}) \approx P(\dot{\gamma}=0)$ signifies that the pressures at nonequilibrium state are approximate to the pressure at equilibrium state. Also, the liquid is very near its Newtonian fluid regime. In contrast, under the extreme shear rate condition of $\dot{\gamma} > 1 \times 10^{11}$ s^{-1}, the pressure rapidly increased with shear rate, which presents shear dilatancy[22–24,28,29] in constant volume NEMD system. Previous studies[22–24,28,29] using NVT-NEMD simulations
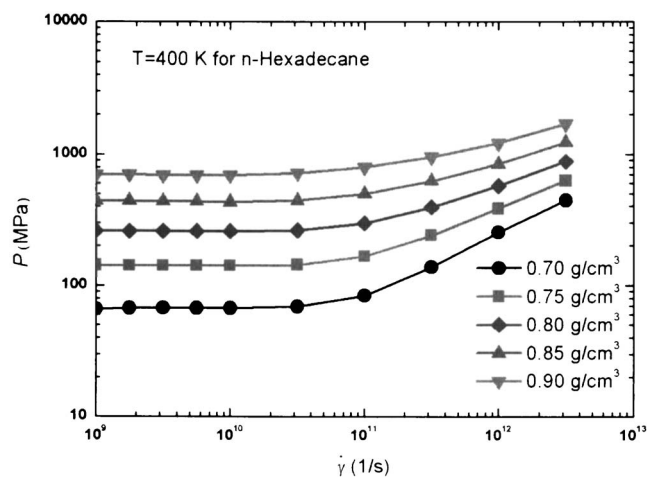
FIG. 14. Shear rate $\dot{\gamma}$ dependence of pressure P for n-hexadecane at 400 K and varying densities obtained by *NVT*-NEMD simulation.

FIG. 15. Pressure P dependence of density ρ for n-hexadecane at 400 K and shear rates of below $1 \times 10^{11.0}$ s^{-1} obtained by *NPT*-NEMD and *NVT*-NEMD simulations and compared with one equilibrium state curve.

have certainly observed nonlinear behavior of nonequilibrium thermodynamic states at high shear rates. In particular, the shear dilatancy results of Kröger *et al.*[24] showed that the pressure decreased with increasing shear rate for long molecular chains consisting of 30–100 FENE beads. They also presented that the pressure increased with increasing shear rate for short chains of ten FENE beads. Therefore, the pressure variation along shear rate increasing depends on the *chain length* and *molecular flexibility*, which is a major difference between FENE or freely jointed chain and realistic alkane fluids, especially for short chain molecules. For long chains, this difference might be expected to disappear.

Many *NVT*-NEMD studies typically show that a *pressure drop* appears between $1 \times 10^{10.5}$ and 1×10^{11} s^{-1}; however, there is no sign of this pressure drop for short molecular chains of $C_{13}H_{28}$ molecules in the study of Daivis *et al.*[23] Also, in the present study for *n*-hexadecane molecules, no sign of a pressure drop in the aforementioned shear rate region was found. While Moore *et al.*[29] observed the pressure drop in simulated long molecular chains of linear $C_{100}H_{202}$ molecules. In detail, Khare *et al.*[28] and Jabbarzadeh *et al.*[31] have presented that linear and branch molecular structures affect the degree of the pressure drop. Their results reveal that long linear chain molecules inevitably induced the pressure drop; however, there was no clear sign of the pressure drop in branch molecules and short linear chain molecules. According to their suggestion, the pressure drop tends to occur as the fluid's molecules reached a minimum energy state of LJ potential.

As seen in Fig. 15, the density-pressure ($\rho - P$) relationship included one equilibrium state curve and some nonequilibrium state points at 400 K. All nonequilibrium state points were extracted from Figs. 12 and 14 under the condition of $\dot{\gamma} < 1 \times 10^{11}$ s^{-1}. At pressures over 500 MPa, state points almost fall on the equilibrium state curve; correspondingly, at pressures below 500 MPa, the densities in *NPT*-NEMD simulation was slightly higher than those in the equilibrium state curve due to statistical errors. As a whole, we suggest that the nonequilibrium state points are close to the equilibrium state curve at $\dot{\gamma} < 1 \times 10^{11}$ s^{-1}.
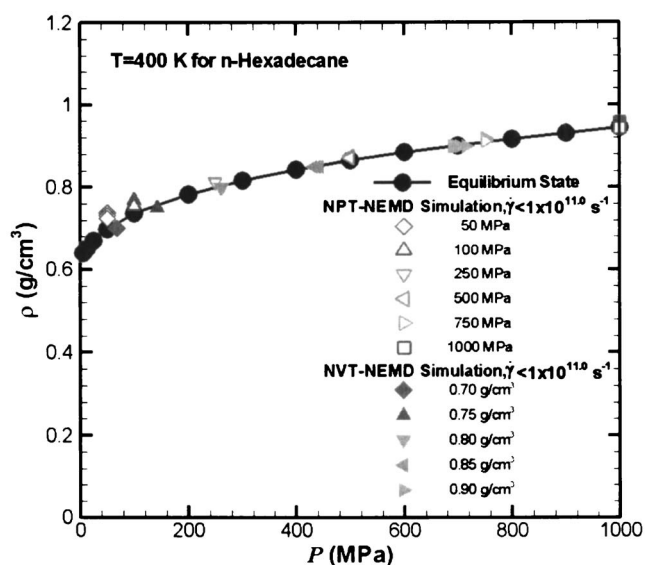
Returning to Fig. 14, the shear dilatancy behavior at $\dot{\gamma} > 1 \times 10^{11.0}$ s^{-1} exhibits the pressure increases with shear rate. To quantify the shear dilatancy behavior in constant volume NEMD simulation, Bosko *et al.* had proposed[42] that the shear dilatancy's P-$\dot{\gamma}$ curve can also be described by the simple power law behavior

$$P(\dot{\gamma}, A_n, n) = A_n \dot{\gamma}^n, \quad \dot{\gamma} > 1 \times 10^{11.0} \text{ s}^{-1}, \tag{28}$$

where A_n is a constant of proportionality, and n is the power law's exponent on shear dilatancy of constant volume NEMD simulation. In general, this exponent is a *positive* value for alkane molecules, which is presented by an increase in pressure with an increase in shear rate.

Figure 16 shows the density dependence of the exponent n. Also, the n value is relative to the degree of shear dilatancy, given by the slope of the P-$\dot{\gamma}$ curve in constant volume NEMD simulation under $\dot{\gamma} > 1 \times 10^{11.0}$ s^{-1} condition.
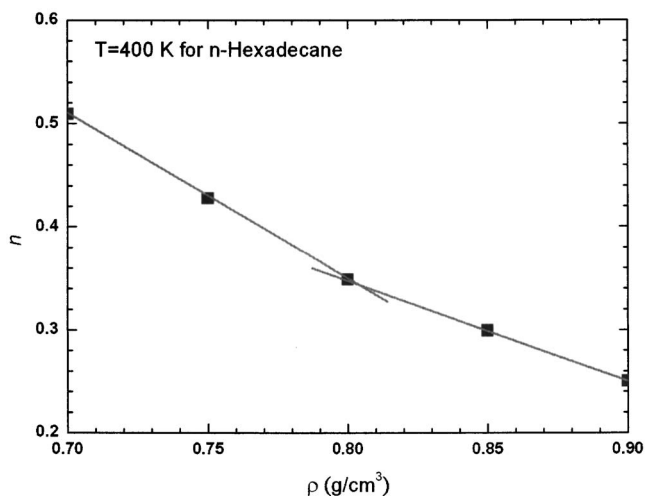

FIG. 16. The power law's exponent n vs density ρ illustrates the dependence of pressure on shear rate for n-hexadecane at 400 K and shear rates of over $1 \times 10^{11.0}$ s^{-1}. Two lines are linear curves fit to the data.

The n variation illustrates that the degree of shear dilatancy decreases with increasing density. An intersection was found near 0.80 g/cm^3. Obviously, the change in shear dilatancy before the intersection was larger than that after the intersection. This finding is similar to the change in shear dilatancy due to the influence of pressure, which also showed a turning point in constant pressure NEMD simulation described in the last section of Sec. III D 2.

E. Variations of shear thinning

The viscosity of a fluid in the liquid phase can be significantly affected by variation in its thermodynamic states (P-ρ-T). Here, we discuss the temperature, pressure, and density induced variation of rheological properties in detail. Key points in this section include analyzing the Newtonian regime's zero-shear-rate viscosity and non-Newtonian regime's shear thinning behavior, as well as using Doolittle's free-volume concept[52] to explain how variation in the viscosity can be affected by the density.

1. Temperature effect

For alkane molecules, the temperature dependence of viscosity can be described via the Arrhenius equation, which indicates that the viscosity decreases as temperature increases,

$$\eta_0(T) = \eta_R \exp\left(\frac{E_a}{RT}\right), \tag{29}$$

where η_R is the reference viscosity, E_a is the flow activation energy, T is the absolute temperature, and R is the gas constant (8.314 J/mol K). In physical terms, the flow activation energy can be thought as an energy barrier of the driven fluid. Once the energy barrier is overcome, the fluid can start to generate the flow behavior. From a molecular viewpoint, the flow activation energy is related to the energy of an alkane molecular as it jumps from one position to another. The intermolecular and intramolecular interaction energies are directly dependent on the flow activation one for alkane molecular.

NPT-NEMD simulation of liquid n-hexadecane at a constant pressure of 250 MPa was used to understand the variation of the viscosity–shear rate (η-$\dot{\gamma}$) flow curves at five different temperatures of 300, 350, 400, 450, and 500 K. Surprisingly, in view of Fig. 17, we found that at over 1 $\times 10^{12.0}$ s^{-1} all η-$\dot{\gamma}$ curves almost overlay each other, which demonstrates the temperature independence of viscosity at the extreme shear rates. At $\dot{\gamma} < 1 \times 10^{12.0}$ s^{-1}, the η-$\dot{\gamma}$ curves at different temperatures show gradual separation, and the viscosity decreases with an increase in temperature.

In the study of Yang *et al.*,[39] 2,2,4,4,6,8,8-heptamethylnonane molecules were analyzed using constant pressure NEMD at 0.1 MPa and different temperatures of 298, 333, and 363 K. Their results show that past the critical shear rate the three η-$\dot{\gamma}$ curves matched each other closely as shear rate increased between $3.0 \times 10^{8.0}$ and $2.4 \times 10^{9.0}$ s^{-1}, which is narrow shear rate region of about one order of magnitude. Similarly, in the present study with a wide shear rate region of $1 \times 10^{9.0}$–$1 \times 10^{12.5}$ s^{-1}, we observe that under ex-

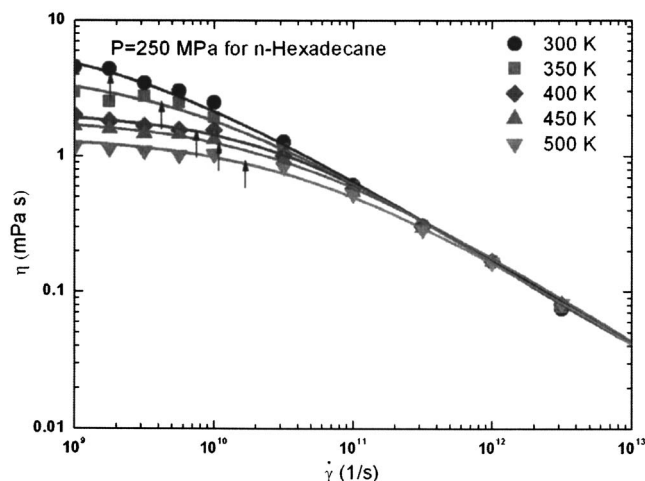FIG. 17. Shear rate $\dot{\gamma}$ dependence of viscosity η for n-hexadecane at 250 MPa and varying temperatures obtained by *NPT*-NEMD simulation. Solid lines are the corresponding Cross model curves fit to η-$\dot{\gamma}$ data. Arrows above indicate critical shear rates.

treme conditions of $\dot{\gamma} < 1 \times 10^{12.0}$ s^{-1} the viscosity is almost independent of temperature. Incidentally, Aoyagi and Doi[40] and Kröger and Hess[41] discussed in detail the chain length induced variation of viscosity. Their results indicated that at extreme shear rates the viscosity is nearly independent on the chain length.

Doolittle's free volume concept[52] is often useful to explain the variation of viscosity with the change in thermodynamic state. This concept describes that the fluid's viscosity decreases with an increase in the free volume of molecules as follows:

$$\eta = A_f \exp(CV_m/V_f), \quad V_f = V - V_m, \tag{30}$$

where A_f and C are constants of proportionality, V is the specific volume, V_m is the specific volume of molecules, and V_f is the free volume of molecules.

As shown in Eq. (30), an incremental increase in the free volume induces a reduction in viscosity. Furthermore, an incremental increase in temperature corresponded to a decrease in density, as seen previously in Fig. 8. Since the density is inversely proportional to volume ($V_f = 1/\rho$), the free volume increases as the density decreases. From a molecular viewpoint, the viscosity directly depends on the mobility or resistance to molecular motion. Therefore, the effect of an increase in the free volume is an increase in the molecular chain's mobility and a decrease in its resistance to motion. Hence, the viscosity decreases as the free volume increases.

In a temperature region of 300–500 K the η-$\dot{\gamma}$ curves contain the Newtonian fluid regime's zero-shear-rate viscosity and the non-Newtonian fluid's shear thinning behavior. First, the extrapolative zero-shear-rate viscosity is determined by the Cross model[8,20,48] of Eq. (25) fitting η-$\dot{\gamma}$ curves. Next, the rotational relaxation time is calculated by the Rouse model of Eq. (26) with the known extrapolative zero-shear-rate viscosity, where equilibrium densities at different temperatures can be obtained from Fig. 8. The critical shear rate is the inverse of the rotational relaxation time. Lastly, the zero-shear-rate viscosity, equilibrium density, ro-

TABLE VI. The temperature dependence of rheological properties at 250 MPa in *NPT*-NEMD simulation.

T (K)	300	350	400	450	500
k	−0.585	−0.541	−0.499	−0.457	−0.412
η_0 (mPa s)	8.251	4.253	2.627	1.895	1.392
ρ (g/cm^3)	0.836	0.818	0.801	0.785	0.770
τ (ps)	543.6	245.5	135.5	88.6	59.7
$\dot{\gamma}_c$ (s^{-1})	1.8×10^9	4.1×10^9	7.4×10^9	1.1×10^{10}	1.7×10^{10}

tational relaxation time, and critical shear rate are arranged in Table VI. As the data shows, the zero-shear-rate viscosity and rotational relaxation time of molecular chains decreased with increasing temperature. This result is consistent with the general physical understanding of polymers.

Returning to Fig. 17, critical shear rates are marked in η-$\dot{\gamma}$ curves. As the temperature increases, it is seen that the zero-shear-rate viscosity falls and the scope of the Newtonian regime widens. To quantify shear thinning behavior, the η-$\dot{\gamma}$ curve in a shear rate region of $1 \times 10^{10.0}$–$1 \times 10^{12.0}$ s^{-1} is described by the power law model[19,48] of Eq. (24). Also, the power law's exponent k for the viscosity is obtained to arrange in Table VI. In addition, for shear thinning the k value is a negative value, which means the viscosity decreases while the shear rate increases. Barbesta *et al.* considered the absolute value of the exponent $|k|$ as the degree of shear thinning.[77] The $|k|$ value is related to the degree of shear thinning, given by the absolute slope of the η-$\dot{\gamma}$ curve in the shear rate region of $1 \times 10^{10.0}$–$1 \times 10^{12.0}$ s^{-1}. Then, the $|k|$−T relationship exhibits the effect of the temperature on shear thinning in Fig. 18. As the temperature increases the degree of the shear thinning linearly decreases, and the scope of the Newtonian regime increases; therefore, viscosity is sensitive to change of temperature.

Further, using the known data of the temperature and zero-shear-rate viscosity in Table VI, the flow activation energy can be found by plotting the relation between log η_0 and 1000/T. The slope of 0.574 for the corresponding curve is shown in Fig. 19. Specifically, we can directly estimate the

flow activation energy, namely, $E_a = \text{slope} \times \ln 10 \times 1000R = 10.99$ kJ/mol via the Arrhenius equation. In this study, the flow activation energy for *n*-hexadecane molecules was predicted at 10.99 kJ/mol. Experimentally, Richard *et al.*[78] measured the flow activation energy for liquid *n*-hexadecane to be 16.0 kJ/mol. In the study of Lee and Chang,[79] who calculated the viscosity and diffusion of alkane molecules by using EMD simulation, the flow activation energy of $C_{12}H_{26}$ molecules was predicted to be 9.74 kJ/mol. Comparatively, the predicted flow activation energy of *n*-hexadecane in this study is an acceptable value.

Eventually, in Sec. III A 1, the heat of vaporization for *n*-hexadecane, using potential model A, was 53.61 kJ/mol. The heat of vaporization represents the activation energy required for a molecular chain to completely exit the liquid phase. By comparing the heat of vaporization and the flow activation energy for *n*-hexadecane, it can be significantly determined that the flow activation energy is about *one-fifth* the heat of vaporization.

2. Pressure effect

For alkane molecules, the pressure dependence of viscosity is described by using Barus's equation,[9,36] which indicates that the viscosity decreases with an increase in pressure,
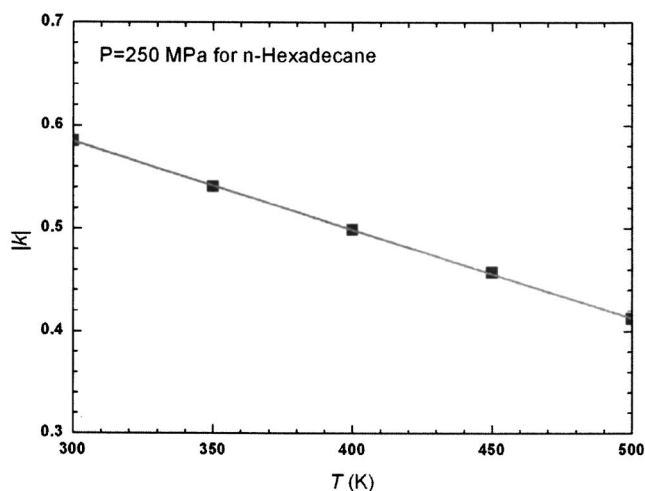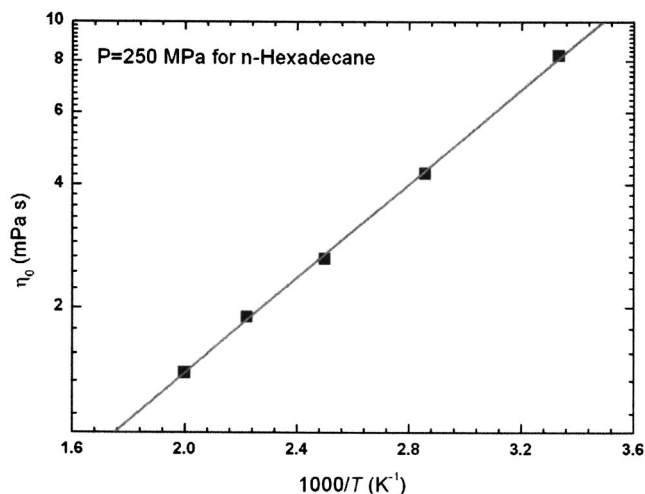

FIG. 18. The absolute value of the power law's exponent $|k|$ vs temperature T illustrates the dependence of viscosity on shear rate for *n*-hexadecane at 250 MPa in a shear rate range of $1 \times 10^{10.0}$–$1 \times 10^{12.0}$ s^{-1}. The line is a linear curve fit to the data.

FIG. 19. Arrhenius' semilog plot of zero-shear-rate viscosity η_0 as a function of temperature T for *n*-hexadecane at 250 MPa. The line is a linear curve fit to the data with a slope of 0.574.
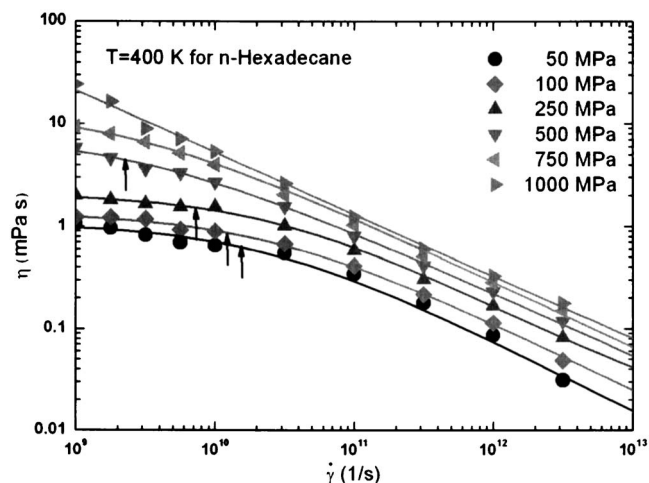
FIG. 20. Shear rate $\dot{\gamma}$ dependence of viscosity η for n-hexadecane at 400 K and varying pressures obtained by NPT-NEMD simulation. Solid lines are the corresponding Cross model curves fit to η-$\dot{\gamma}$ data. Arrows above indicate critical shear rates.

FIG. 21. The absolute value of the power law's exponent $|k|$ vs pressure P illustrates the dependence of viscosity on shear rate for n-hexadecane at 400 K in a shear rate range of $1 \times 10^{10.0}$–$1 \times 10^{12.0}$ s^{-1}. The two lines are linear curves fit to the data.

$$\eta_0(T, P) = \eta_{\text{atm}} \exp(\alpha(T)P), \qquad (31)$$

where η_{atm} is the viscosity at atmospheric pressure and $\alpha(T)$ is the pressure-viscosity coefficient, which is dependent on temperature.

First, using NPT-NEMD simulation of liquid n-hexadecane at a constant temperature of 400 K, the variation of the η-$\dot{\gamma}$ flow curve at six different pressures of 50, 100, 250, 500, 750, and 1000 MPa was analyzed. As shown in Fig. 20, the incremental change in viscosity with increasing pressure agrees well with the relation of Barus' equation. Additionally, by using Doolittle's free volume concept, the density increase resulted in a decrease of the free volume with increasing pressure as seen in Fig. 11. The increase in viscosity with the corresponding increase in pressure is due to the decline in mobility of the molecular chains.

Next, between 50 and 500 MPa, the η-$\dot{\gamma}$ flow curves pass from the Newtonian regime to the non-Newtonian regime. As the pressure increased, the Newtonian regime's scope decreased. Clearly, under extreme pressure conditions of 750 and 1000 MPa, it is seen that there is almost no sign of the Newtonian plateau in the fitted curves of Fig. 20. As seen in last section of Sec. III E 1, by using the Cross model, the power law model, and the Rouse model, the zero-shear-rate viscosity, rotational relaxation time, critical shear rate, as well as the power law's exponent have been arranged in Table VII. Also, at different pressures, equilibrium densities can be obtained from Fig. 11. As shown in Table VII, the zero-shear-rate viscosity and rotational relaxation time of
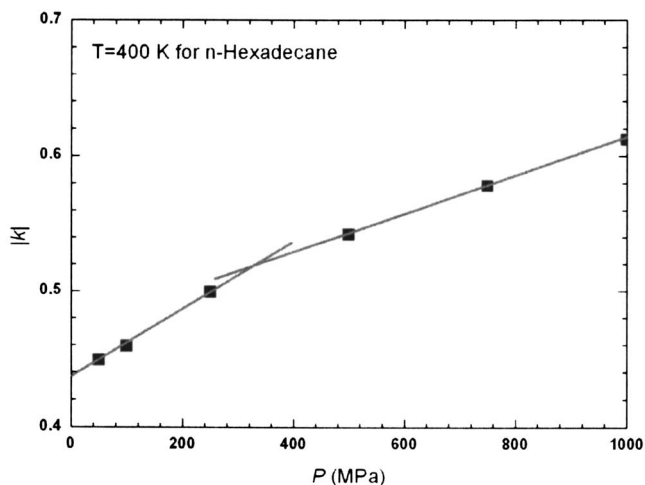
molecular chains increase with increasing pressure. This result and the understanding of polymer physics match pretty well.

Returning to Fig. 20, arrows indicate the critical shear rates on the η-$\dot{\gamma}$ curves, and signify the onset of shear thinning. By reviewing the inflection points marked on the η-$\dot{\gamma}$ curves, we clearly observe that in a constant shear rate region the Newtonian regime's scope decreases and the shear thinning behavior's scope increases with an increase in pressure.

Moreover, Fig. 21 shows the pressure dependence of the absolute value of the power law's exponent ($|k|$–P) for the viscosity. As pressure increases, the degree of shear thinning $|k|$ increases and the Newtonian regime's scope decreases. Additionally, an *intersection* was found near 320 MPa by fitting two linear curves to the data. The change in the degree of shear thinning before the intersection is larger than after the intersection; consequently, the shear thinning behavior at pressures below 320 MPa is stronger than at pressures over 320 MPa. In this study the observation of pressures affect on the variation of the η-$\dot{\gamma}$ curves is clearly shown as the pressure region is *pretty wide*. Over a narrow pressure region, the variation of the η-$\dot{\gamma}$ curves would not be easily discernible.

Finally, using the known data of the pressure and the zero-shear-rate viscosity shown in Table VII, the pressure-viscosity coefficient α can be determined by plotting the relation between log η_0 and P. In Fig. 22, the slope of the resulting curve equals 0.001 92 MPa^{-1} such that the pressure-viscosity coefficient $\alpha = \ln 10 \times \text{slope} = 4.42$ GPa^{-1}.

TABLE VII. The pressure dependence of rheological properties at 400 K in NPT-NEMD simulation.

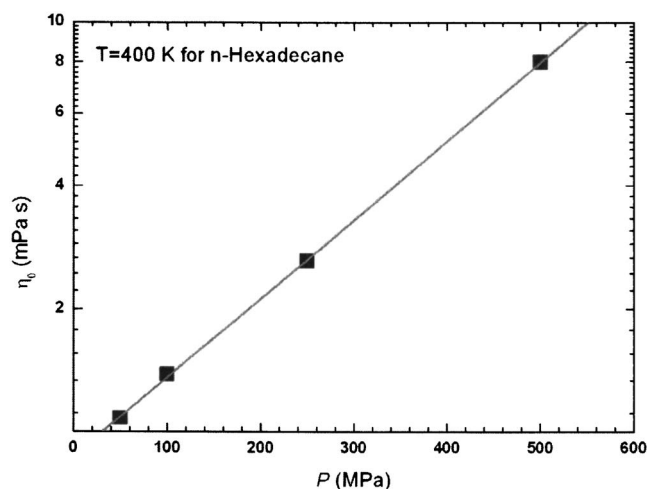| P (MPa)	50	100	250	500	750	1000
k	−0.449	−0.459	−0.499	−0.542	−0.578	−0.612
η_0 (mPa s)	1.081	1.384	2.627	8.013	⋯	⋯
ρ (g/cm^3)	0.699	0.737	0.801	0.866	⋯	⋯
τ (ps)	63.9	77.6	135.5	382.2	⋯	⋯
$\dot{\gamma}_c$ (s^{-1})	1.6×10^{10}	1.3×10^{10}	7.4×10^9	2.6×10^9	⋯	⋯

FIG. 22. Barus' semilog plot of zero-shear-rate viscosity η_0 as a function of pressure P for n-hexadecane at 400 K. The line is a linear curve fit to the data with a slope of 0.001 92.

FIG. 23. Shear rate $\dot{\gamma}$ dependence of viscosity η for n-hexadecane at 400 K and varying densities obtained by NVT-NEMD simulation. Solid lines are the corresponding Cross model curves fit to η-$\dot{\gamma}$ data. Arrows above indicate critical shear rates.

As the pressure-viscosity coefficient must be measured at extreme pressure states, the amount of experimental data for the pressure-viscosity coefficient is limited in practice. In general, the pressure-viscosity coefficient[20] is about $1-30$ GPa^{-1} in lubrication processes. The study of McCabe et $al.$,[36] which performed NVT-NEMD simulation on starlike molecules of $C_{25}H_{52}$, shows that at 372.04 K the pressure-viscosity coefficient is approximately 5.88 GPa^{-1}. Although the molecular structure and simulation temperature are different, our estimated value of the pressure-viscosity coefficient for n-hexadecane molecules is a reasonable value as compared to their results.

3. Density effect

In the final section, by using NVT-NEMD simulation of liquid n-hexadecane at a constant temperature of 400 K, we observe the variation of the η-$\dot{\gamma}$ flow curves at five different densities of 0.70, 0.75, 0.80, 0.85, and 0.90 g/cm^3. As shown in Fig. 23, there is an incremental increase in viscosity at increased density. According to Doolittle's free volume concept, the density increase will result in a decrease in the free volume of molecules. As expected, with a decline in the mobility of molecular chains, the viscosity increased. As seen in last section of Sec. III E 2, an increase in pressure results in an increase in viscosity. Also, the density effect is quite similar to the pressure effect.

Between 0.70 and 0.75 g/cm^3, the η-$\dot{\gamma}$ flow curves move along the Newtonian regime to the non-Newtonian regime. As the density increased slightly, the Newtonian reg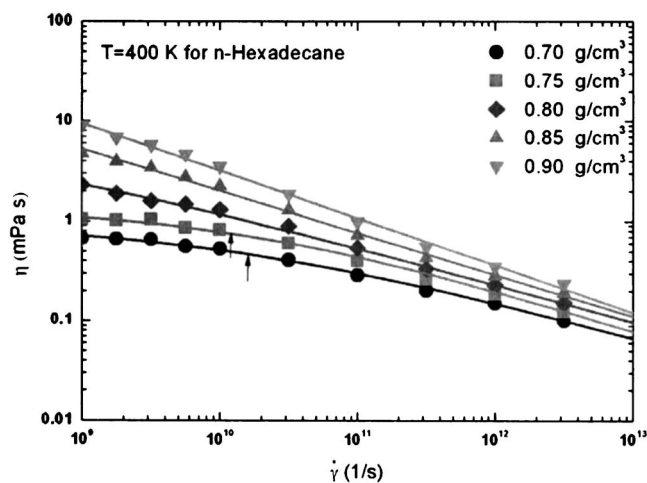ime's scope decreased rapidly. As the density approached 0.80 g/cm^3, the Newtonian regime's scope almost vanished. At higher densities of 0.85 and 0.90 g/cm^3, there was no sign of the Newtonian plateau in the η-$\dot{\gamma}$ flow curves. Referring back to the discussion presented in Sec. III E 1, both Cross and power law models can be used to fit the η-$\dot{\gamma}$ flow curves to the data. In addition, the rotational relaxation time is calculated by the Rouse model of Eq. (26) with the zero-shear-rate viscosity. At different densities, the zero-shear-rate viscosity, rotational relaxation time, critical shear rate, as well as the power law's exponent are arranged in Table VIII. Consequently, the zero-shear-rate viscosity and rotational relaxation time of the molecular chains increased with density. This result is qualitatively consistent with the physical perspective of polymers.

In Fig. 23, arrows are marked on the η-$\dot{\gamma}$ curves to reveal the critical shear rate, and subsequently the starting point of shear thinning. A review of the location of the arrow on the curves indicated that in a constant shear rate region the Newtonian regime's scope decreases and the shear thinning behavior's scope increases with increase in density.

Eventually, Fig. 24 shows the density dependence of the absolute value of the power law's exponent on the viscosity ($|k|-\rho$). As the density increased from 0.70 to 0.90 g/cm^3, the degree of shear thinning $|k|$ linearly increased from 0.280 to 0.506, and the Newtonian regime's scope strongly decreased. Obviously, the change in viscosity is sensitive to the small change in density as compared to the effects of changes in the pressure and temperature.

TABLE VIII. The density dependence of rheological properties at 400 K in NVT-NEMD simulation.

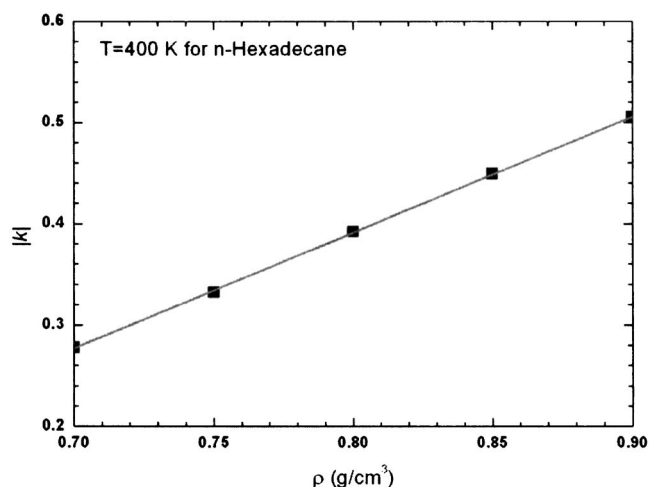| ρ (g/cm^3)	0.70	0.75	0.80	0.85	0.90
k	-0.278	-0.332	-0.392	-0.449	-0.505
η_0 (mPa s)	0.992	1.423	$\cdots$	$\cdots$	$\cdots$
τ (ps)	58.5	78.4	$\cdots$	$\cdots$	$\cdots$
$\dot{\gamma}_e$ (s^{-1})	1.7×10^{10}	1.3×10^{10}	$\cdots$	$\cdots$	$\cdots$

FIG. 24. The absolute value of the power law's exponent $|k|$ vs density ρ illustrates the dependence of viscosity on shear rate for n-hexadecane at 400 K in a shear rate range of $1 \times 10^{10.0}$–$1 \times 10^{12.0}$ s^{-1}. The line is a linear curve fit to the data.

IV. CONCLUSIONS

We have reported a series of results for thermodynamic states and rheological properties of liquid n-hexadecane molecules through equilibrium and nonequilibrium molecular dynamics (EMD and NEMD) simulations, including constant volume NEMD (*NVT*-NEMD) and constant pressure NEMD (*NPT*-NEMD) systems. By using two different potential models, the qualitative descriptions of the properties are similar in nature to the observed physical behaviors. In addition, the comparison between quantitative predictions and experimental data depend on the potential models utilized.

At present, we have confirmed that shear rate directly affects thermodynamic state, pressure-density-temperature P-ρ-T data. A transition point affecting P-ρ-T data occurs at a shear rate $\dot{\gamma} \approx 1 \times 10^{11.0}$ s^{-1}. Further, at $\dot{\gamma} < 1 \times 10^{11.0}$ s^{-1} we observed that nonequilibrium thermodynamic states are close to equilibrium ones, which indicate that the fluid is nearly into its Newtonian fluid regime. In contrast, at higher shear rates of over $1 \times 10^{11.0}$ s^{-1} the thermodynamic state curves show the important nonlinear behavior of shear dilatancy. At $\dot{\gamma} > 1 \times 10^{11.0}$ s^{-1} the shear dilatancy behaviors were presented with increases in shear rate as shown by decreased density and increased pressure through *NPT*-NEMD and *NVT*-NEMD simulations, respectively. In *NPT*-NEMD simulation we suggested that the degree of shear dilatancy increased linearly as temperatures increased, and decreased as pressure increased. In particular, after a turning point occurred between 100 and 250 MPa, the slope change in shear dilatancy with increasing pressure slowly decreases and nearly approaches a constant value at over 1000 MPa. Additionally, through *NVT*-NEMD simulation it has been shown that the degree of the shear dilatancy falls as the density rises.

From a rheological viewpoint, the viscosity–shear rate (η-$\dot{\gamma}$) flow curve consists of the zero-shear-rate viscosity in the fluid's Newtonian regime and shear thinning behavior in the non-Newtonian regime. By both Cross and power law models fitting to the η-$\dot{\gamma}$ flow curve, we can gain the ex-

trapolated zero-shear-rate viscosity in the Newtonian regime and the power law's exponent in the shear thinning regime, respectively. The rotational relaxation time of n-hexadecane was calculated by using Rouse model with the zero-shear viscosity, and the critical shear rate, which is the inverse of the rotational relaxation time, indicated the transition point from Newtonian to non-Newtonian behavior. The critical shear rate marked on the η-$\dot{\gamma}$ flow curve is in approximate agreement with the observed NEMD simulation data. Expectably, the zero-shear-rate viscosity and rotational relaxation time decrease with increasing temperature. As the pressure or density increases, the zero-shear-rate viscosity and rotational relaxation time increase. This result is qualitatively consistent with our understanding of polymer physics.

As focused in a constant shear rate region of *NPT*-NEMD simulation, the scope of the Newtonian region increases and the scope of the shear thinning region decreases with increase in temperature. Especially, at extreme shear rates over $1 \times 10^{12.0}$ s^{-1} the viscosity is almost independent of temperature. Conversely, at shear rates below $1 \times 10^{12.0}$ s^{-1}, the viscosity decreases with increasing temperature. The temperature dependence of the zero-shear-rate viscosity is described by the Arrhenius equation. We measured the flow activation energy of 10.99 kJ/mol, which is in reasonable agreement with the predicted value of MD simulation and related experimental data. Also, the flow activation energy is about one-fifth the heat of vaporization.

Furthermore, as the pressure increases the scope of the Newtonian region decreases and the scope of the shear thinning region increases. When the pressure reaches extreme values of 750 and 1000 MPa, the Newtonian region vanishes completely. This shows explicitly that the non-Newtonian behavior of shear thinning occurs strongly at high pressure. The pressure dependence of the zero-shear-rate viscosity is described by the Barus equation. It is a reasonable prediction that the pressure-viscosity coefficient of n-hexadecane at 400 K gained 4.22 GPa^{-1} in the analysis of the present study.

Moreover, from the results of *NVT*-NEMD simulation, the Newtonian region's scope decreases and the shear thinning region's scope increases with increasing density. As the density is over 0.80 g/cm^3, the Newtonian region was not observed. Thus, the viscosity was sensitive to slightly varied density. Surely, our simulation is able to explain the change in viscosity with variations of thermodynamic state and is in good agreement with Doolittle's free volume concept.

As this study has shown, it is useful to understand shear rate's effect on the fluid's thermodynamic state, as well as the influence of the temperature, pressure, and density on the η-$\dot{\gamma}$ relationship. As a whole, the qualitative predications are in close agreement with rheological perspective. In the limitation of this study, convergence of the viscosity required significant central processing unit (CPU) time at very lower shear rates due to the occurrence of thermonoise resulting to statistical errors. However, this issue has been solved by Evans and Morriss, who proposed a method using the transient time correlation function[8,11,80] (TTCF). Recently, a lowest shear rate of $1 \times 10^{5.0}$ s^{-1} in NEMD simulation has been reached by applying the TTCF method.[8,80] Before long, we will further utilize this method to gain a confirmable value of

the zero-shear-rate viscosity in a wide Newtonian plateau. Also, the affect of molecular chain's length on shear thinning will be discussed by adopting this method, which requires significant CPU time for long molecular chains to converge.

In conclusion, the MD simulation technologies developed in the present study show significant correlation to qualitative, experimental, and other MD studies, which make them an excellent valuable tool in the fundamental thermodynamic and rheological researches. In future studies, from molecular perspective we will further extend our simulation systems to analyze molecular chain's structure characteristics of the end-to-end distance, gyration radius, and orientation order of molecular chains to broaden the understanding of the thermodynamic state variation's effect on shear dilatancy and shear thinning.

ACKNOWLEDGMENTS

[1] J. N. Israelachvili, P. M. Mcguiggan, and A. M. Homola, Science **240**, 189 (1988).
[2] B. Bhushan, J. N. Israelachvili, and U. Landman, Nature (London) **374**, 607 (1995).
[3] G. Carson, H.-W. Hu, and S. Granick, Tribol. Trans. **35**, 405 (1992).
[4] Y.-Z. Hu and S. Granick, Tribol. Lett. **5**, 81 (1998).
[5] M. P. Allen and J. Tildesley, *Computer Simulation of Liquid* (Oxford University Press, New York, 1989).
[6] S. T. Cui, P. T. Cummings, and H. D. Cochran, Mol. Phys. **93**, 117 (1998).
[7] J. J. Erpenbeck, Phys. Rev. A **38**, 6255 (1988).
[8] G. Pan and C. McCabe, J. Chem. Phys. **125**, 194527 (2006).
[9] R. C. Coy, Tribol. Int. **31**, 563 (1998).
[10] R. Edberg, G. P. Morriss, and D. J. Evans, J. Chem. Phys. **86**, 4555 (1987).
[11] D. J. Evans and G. P. Morriss, *Statistical Mechanics of Nonequilibrium Liquids* (Academic, London, 1990).
[12] B. D. Todd and P. J. Daivis, Mol. Simul. **33**, 189 (2007).
[13] A. Berker, S. Chynoweth, U. C. Klomp, and Y. Michopoulos, J. Chem. Soc., Faraday Trans. **88**, 1719 (1992).
[14] D. J. Evans, G. P. Morriss, and L. M. Hood, Mol. Phys. **68**, 637 (1989).
[15] B. Busic, J. Koplik, and J. R. Banavar, J. Non-Newtonian Fluid Mech. **109**, 51 (2003).
[16] P. J. Daivis, M. L. Matin, and B. D. Todd, J. Non-Newtonian Fluid Mech. **111**, 1 (2003).
[17] J. G. H. Cifre, S. Hess, and M. Kröger, Macromol. Theory Simul. **13**, 748 (2004).
[18] J. D. Moore, S. T. Cui, H. D. Cochran, and P. T. Cummings, J. Non-Newtonian Fluid Mech. **93**, 101 (2000).
[19] S. Chynoweth and Y. Michopoulos, Mol. Phys. **81**, 133 (1994).
[20] S. Chynoweth, R. C. Coy, and Y. Michopoulos, Proc. Inst. Mech. Eng., Part J: J. Eng. Tribol. **209**, 243 (1995).
[21] D. J. Evans and G. P. Morriss, Phys. Rev. Lett. **56**, 2172 (1986).
[22] L. M. Hood, D. J. Evans, and J. M. Hanley, J. Stat. Phys. **57**, 729 (1989).
[23] P. J. Daivis, D. J. Evans, and G. P. Morriss, J. Chem. Phys. **97**, 616 (1992).
[24] M. Kröger, W. Loose, and S. Hess, J. Rheol. **37**, 1057 (1993).
[25] P. J. Daivis and D. J. Evans, J. Chem. Phys. **100**, 541 (1994).
[26] C. J. Mundy, J. L. Siepmann, and M. L. Klein, J. Chem. Phys. **103**, 10192 (1995).
[27] Z. Xu, J. J. de Pablo, and S. Kim, J. Chem. Phys. **102**, 5836 (1995).
[28] R. Khare, J. J. de Pablo, and A. Yethiraj, J. Chem. Phys. **107**, 6956 (1997).
[29] J. D. Moore, S. T. Cui, H. D. Cochran, and P. T. Cummings, J. Non-Newtonian Fluid Mech. **93**, 83 (2000).
[30] J. Delhommelle and D. J. Evans, J. Chem. Phys. **115**, 43 (2001).
[31] A. Jabbarzadeh, J. D. Atkinson, and R. I. Tanner, Macromolecules **36**, 5020 (2003).
[32] P. Padilla and S. Toxvaerd, J. Chem. Phys. **97**, 7687 (1992).
[33] S. T. Cui, P. T. Cummings, and H. D. Cochran, J. Chem. Phys. **104**, 255 (1996).
[34] S. T. Cui, S. A. Gupta, and P. T. Cummings, J. Chem. Phys. **105**, 1214 (1996).
[35] J. D. Moore, S. T. Cui, H. D. Cochran, and P. T. Cummings, J. Chem. Phys. **113**, 8833 (2000).
[36] C. McCabe, S. Cui, P. T. Cummings, P. A. Gordon, and R. B. Saeger, J. Chem. Phys. **114**, 1887 (2001).
[37] S. Bair, C. McCabe, and P. T. Cummings, Phys. Rev. Lett. **88**, 058302 (2002).
[38] C. McCabe, C. W. Manke, and P. T. Cummings, J. Chem. Phys. **116**, 3339 (2002).
[39] Y. Yang, T. A. Pakkanen, and R. L. Rowley, Int. J. Thermophys. **23**, 1441 (2002).
[40] T. Aoyagi and M. Doi, Comput. Theor. Polym. Sci. **10**, 317 (2000).
[41] M. Kröger and S. Hess, Phys. Rev. Lett. **85**, 1128 (2000).
[42] J. T. Bosko, B. D. Todd, and R. J. Sadus, J. Chem. Phys. **121**, 12050 (2004).
[43] J. T. Bosko, B. D. Todd, and R. J. Sadus, J. Chem. Phys. **123**, 034905 (2005).
[44] V. K. Gupta, R. Sureshkumar, and B. Khomami, Phys. Fluids **16**, 1546 (2004).
[45] M. Doi and S. F. M. Edwards, *The Theory of Polymer Dynamics* (Clarendon, Oxford, 1986).
[46] Y.-H. Lin, *Polymer Viscoelasticity* (World Scientific, London, 2003).
[47] R. B. Bird, R. C. Armstrong, and O. Hassager, *Fluid Mechanics*, Dynamics of Polymeric Liquids, Vol. 1, 2nd ed. (Wiley-Interscience, New York, 1987).
[48] H. A. Barnes, J. F. Hutton, and K. Walters, *An Introduction to Rheology* (Elsevier, New York, 1989).
[49] R. I. Tanner, *Engineering Rheology* (Oxford University Press, New York, 1989).
[50] J.-C. Wang and K. A. Fichthorn, J. Chem. Phys. **109**, 10138 (1998).
[51] R. B. Bird, R. C. Armstrong, and O. Hassager, *Kinetic Theory*, Dynamics of Polymeric Liquids, Vol. 2, 2nd ed. (Wiley-Interscience, New York, 1987).
[52] M. T. Shaw and W. J. MacKnight, *Introduction to Polymer Viscoelasticity*, 3rd ed. (Wiley-Interscience, Hoboken, 2005).
[53] A. Jabbarzadeh, J. D. Atkinson, and R. I. Tanner, J. Non-Newtonian Fluid Mech. **77**, 53 (1998).
[54] M. J. Stevens, M. Mondello, G. S. Grest, S. T. Cui, H. D. Cochran, and P. T. Cummings, J. Chem. Phys. **106**, 7303 (1997).
[55] H.-C. Tseng, J.-S. Wu, and R.-Y. Chang, "Molecular dynamics simulation of short-chain polyethylene in a nano-contraction flow," Phys. Fluids (submitted).
[56] D. N. J. White and M. J. Bovill, J. Chem. Soc., Perkin Trans. 2 **1977**, 1610.
[57] J.-P. Ryckaert and A. Bellemans, Chem. Phys. Lett. **30**, 123 (1975).
[58] M. G. Martin and J. L. Siepmann, J. Phys. Chem. B **102**, 2569 (1998).
[59] J. López-Lemus, M. Romero-Bastida, T. A. Darden, and J. Alejandre, Mol. Phys. **104**, 2413 (2006).
[60] J. I. Siepmann, S. Karaborni, and B. Smit, Nature (London) **365**, 330 (1993).
[61] J. P. Nicolas and B. Smit, Mol. Phys. **100**, 2471 (2002).
[62] J. M. Haile, *Molecular Dynamics Simulation*, 2nd ed. (Wiley-Interscience, New York, 1997).
[63] W. L. Jorgensen, J. D. Madura, and C. J. Swenson, J. Am. Chem. Soc. **106**, 6638 (1984).
[64] A. W. Lees and S. F. Edwards, J. Phys. C **5**, 1921 (1972).
[65] K. P. Travis, P. J. Daivis, and D. J. Evans, J. Chem. Phys. **103**, 1109 (1995).
[66] D. Macgowan and D. M. Heyes, Mol. Simul. **1**, 277 (1988).
[67] S. Chynoweth, U. C. Klomp, and L. E. Scales, Comput. Phys. Commun. **62**, 297 (1991).
[68] J. H. Irving and J. G. Kirkwood, J. Chem. Phys. **18**, 817 (1950).
[69] J. E. Carpenter, J. Comput. Chem. **23**, 667 (2002).
[70] H. W. Horn, W. C. Swope, J. W. Piter, J. D. Madura, T. J. Dick, G. L. Hura, and T. Head-Gordon, J. Chem. Phys. **120**, 9665 (2004).
[71] Research Committee on Lubrication, *Pressure-Viscosity Report* (American Society of Mechanical Engineers, New York, 1953), Vol. II.
[72] E. W. Lemmon, M. O. McLinden, and D. G. Friend, in *NIST Chemistry*

WebBook, edited by P. J. Linstrom and W. G. Mallard (National Institute of Standards and Technology, Gaithersburg MD, 2005) (http://webbook.nist.gov).

[73] S. K. Nath, F. A. Escobedo, and J. J. de Pablo, J. Chem. Phys. **108**, 9905 (1998).

[74] J. Chang and S. I. Sandler, J. Chem. Phys. **121**, 7474 (2004).

[75] M. J. Anselme, M. Gude, and A. S. Teja, Fluid Phase Equilib. **57**, 317 (1990).

[76] P. E. Rouse, J. Chem. Phys. **21**, 1272 (1953).

[77] F. Barbesta, D. W. Bousfield, and M. Rigdahl, J. Rheol. **45**, 139 (2001).

[78] R. C. Dorrance, T. F. Hunter, and J. Philp, J. Chem. Soc., Faraday Trans. 2 **73**, 89 (1977).

[79] S. H. Lee and T. Chang, Bull. Korean Chem. Soc. **24**, 1590 (2003).

[80] I. Borzsák, P. T. Cummings, and D. J. Evans, Mol. Phys. **100**, 2735 (2002).